Article

Cell Reports

SNAREs Controlling Vesicular Release of BDNF and Development of Callosal Axons

Graphical Abstract

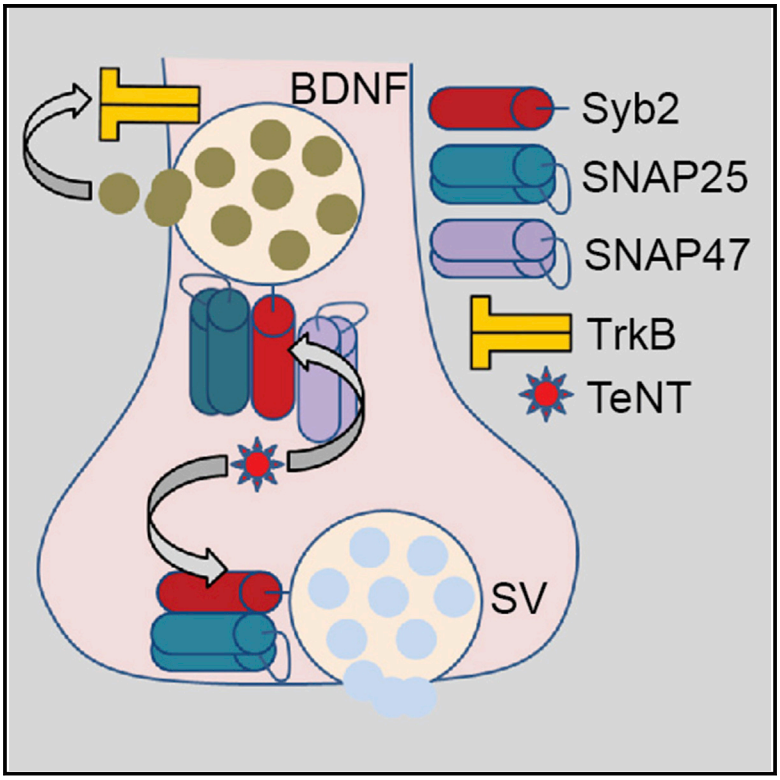

Authors

Masafumi Shimojo, Julien Courchet, ..., Franck Polleux, Anton Maximov

Correspondence

amaximov@scripps.edu

In Brief

Shimojo et al. investigated mechanisms of protein secretion in central neurons. They identified SNAREs that drive the vesicular exocytosis of BDNF, a secreted factor involved in neural circuit development and plasticity. Loss of BDNF or SNAREs that promote BDNF release in callosal cortical neurons impairs the development of their axons.

Highlights

- BDNF is a secreted protein that regulates neuronal development and plasticity
- Vesicular exocytosis of BDNF is driven by SNAREs, Syb2, SNAP25, and SNAP47
- Unlike Syb2 and SNAP25, SNAP47 appears to be unnecessary for neurotransmission
- Loss of BDNF or SNAP47 in callosal neurons diminishes branching of their axons

Shimojo et al., 2015, Cell Reports *11*, 1–13
May 19, 2015
http://dx.doi.org/10.1016/j.celrep.2015.04.032

CellPress

Please cite this article in press as: Shimojo et al., SNAREs Controlling Vesicular Release of BDNF and Development of Callosal Axons, Cell Reports (2015), http://dx.doi.org/10.1016/j.celrep.2015.04.032

Cell Reports
Article

SNAREs Controlling Vesicular Release of BDNF and Development of Callosal Axons

Masafumi Shimojo,[1,2,4] Julien Courchet,[1,2,5] Simon Pieraut,[1,2] Nina Torabi-Rander,[1,2] Richard Sando III,[1,2,3] Franck Polleux,[1,2,5] and Anton Maximov[1,2,*]

[1]Department of Molecular and Cellular Neuroscience, The Scripps Research Institute (TSRI), La Jolla, CA 92037, USA
[2]The Dorris Neuroscience Center (DNC), The Scripps Research Institute (TSRI), La Jolla, CA 92037, USA
[3]The Kellogg School of Science and Technology, The Scripps Research Institute (TSRI), La Jolla, CA 92037, USA
[4]Present address: Molecular Imaging Center, National Institute of Radiological Sciences, Chiba 263-8555, Japan
[5]Present address: Department of Neuroscience, Zuckerman Mind Brain Behavior Institute and Kavli Institute for Brain Science, Columbia University, New York, NY 10032, USA
*Correspondence: amaximov@scripps.edu
http://dx.doi.org/10.1016/j.celrep.2015.04.032

SUMMARY

At presynaptic active zones, exocytosis of neurotransmitter vesicles (SVs) is driven by SNARE complexes that recruit Syb2 and SNAP25. However, it remains unknown which SNAREs promote the secretion of neuronal proteins, including those essential for circuit development and experience-dependent plasticity. Here we demonstrate that Syb2 and SNAP25 mediate the vesicular release of BDNF in axons and dendrites of cortical neurons, suggesting these SNAREs act in multiple spatially segregated secretory pathways. Remarkably, axonal secretion of BDNF is also strongly regulated by SNAP47, which interacts with SNAP25 but appears to be dispensable for exocytosis of SVs. Cell-autonomous ablation of SNAP47 disrupts the layer-specific branching of callosal axons of projection cortical neurons in vivo, and this phenotype is recapitulated by ablation of BDNF or its receptor, TrkB. Our results provide insights into the molecular mechanisms of protein secretion, and they define the functions of SNAREs in BDNF signaling and regulation of neuronal connectivity.

INTRODUCTION

Neurons activated during experience may nearly simultaneously release fast neurotransmitters and diffusible polypeptides from distinct membrane-trafficking organelles. Synaptic neurotransmitter vesicles (SVs) reside at axon terminals and undergo exocytosis at highly compartmentalized active zones, whereas peptidergic vesicles are broadly distributed in axons and dendrites (Dean et al., 2012; Südhof, 2013). The core presynaptic release machinery includes SNAREs, synaptobrevin/VAMP2 (Syb2), SNAP25, and syntaxin1, whose assembly into ternary complexes primes SVs for rapid exocytosis and overcomes the energy barrier for their fusion with the plasma membrane (Schoch et al., 2001; Südhof and Rothman, 2009; Wojcik and Brose, 2007). These SNAREs play similar roles in the release of catecholamines from dense core vesicles (DCVs) in chromaffin cells and promote membrane fusion in vitro (Giraudo et al., 2009; Sakaba et al., 2005; Sørensen et al., 2003b), which supports the hypothesis that SNAREs universally control secretion. Surprisingly, the contribution of SNAREs to secretion of neuronal proteins is largely unexplored. Moreover, invertebrate and vertebrate genomes have relatively few VAMPs and SNAPs, which raises the following question: to what extent are individual SNARE isoforms shared in a given neuron between organelles with different content?

These gaps in knowledge of the basic aspects of membrane trafficking present a challenge for understanding the mechanisms of experience-dependent plasticity at molecular and circuit levels. For example, experimental evidence suggests that both neurotransmitters and peptides may influence axon branching and patterning of synaptic networks of various neuron classes (Bloodgood et al., 2013; Cao et al., 2007; Cheng et al., 2011; Kerschensteiner et al., 2009; Pieraut et al., 2014; Wang et al., 2007; Yu et al., 2004). Yet, virtually all contemporary methods for pharmacological, genetic, or optogenetic control of network activity in live animals likely affect secretion in a non-selective manner, making it difficult to define the impacts of specific cues on neural circuit structure, function, and, ultimately, animal behavior. Likewise, cleavage of Syb2 with genetically encoded tetanus toxin (TeNT) has become a popular approach for blocking exocytosis of SVs (Kerschensteiner et al., 2009; Pieraut et al., 2014; Wang et al., 2007; Yu et al., 2004), but it remains unclear how TeNT affects other vesicle types. Although these problems can be partially overcome by ablating neurotransmitter or peptide-specific receptors, such strategies have a limited use for the identification of cellular sources of release.

The brain-derived neurotrophic factor (BDNF) has emerged as one of the key diffusible signals that is essential for axon growth, synaptogenesis, remodeling of mature synapses, learning, and memory (Lu et al., 2013; Park and Poo, 2013).

Please cite this article in press as: Shimojo et al., SNAREs Controlling Vesicular Release of BDNF and Development of Callosal Axons, Cell Reports (2015), http://dx.doi.org/10.1016/j.celrep.2015.04.032

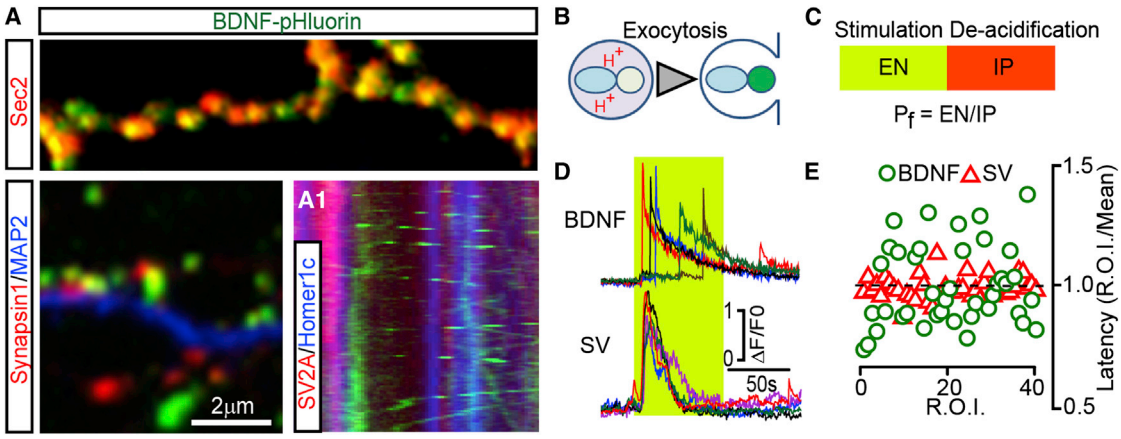

Figure 1. Intracellular Trafficking and Exocytosis of BDNF Vesicles

(A) DIV15 neurons expressing BDNF-pHluorin from a lentivirus were labeled with antibodies to GFP (as a probe for BDNF construct) and markers of either peptidergic (Sec2, top) or neurotransmitter vesicles (Synapsin1, bottom left). MAP2 labels dendrites. (Bottom right) Kymograph from time-lapse imaging of live neurons co-expressing BDNF-GFP and reporters of presynaptic terminals and dendritic spines, tdTomato-SV2A and EBFP2-Homer1c. See also Figures S1 and S2.

(B) Schematic shows reporter de-acidification during vesicle fusion with the plasma membrane.

(C) A protocol for quantitative analysis of exocytosis.

(D and E) Exocytosis of BDNF and SVs was monitored at DIV15 by time-lapse TIRF imaging of BDNF-pHluorin and SyP-pHluorin, respectively. (D) Sample traces reflecting fusion in different sites of the same neuron during direct depolarization with KCl (50 mM). Green box marks the time course of intracellular calcium rise, as determined in identical experimental settings in neurons expressing GCaMP3. (E) Latencies of isolated fusion events are plotted as ratios to averaged latency per cell (n = 4, 10 sites/neuron). See also Figure S2, Movies S1, S2, S3, and S4, and Supplemental Experimental Procedures.

While secretion of native neurotrophins is notoriously difficult to detect in real time, it is generally agreed that BDNF is transported by secretogranin2-positive vesicles that undergo exocytosis upon synaptic excitation and calcium influx (de Wit et al., 2009; Dean et al., 2012; Dieni et al., 2012; Kolarow et al., 2007; Matsuda et al., 2009; Sadakata et al., 2012, 2013). Structurally, the axonal pool of these organelles resembles DCVs, whereas dendritic vesicles do not have characteristic dense cores (Dieni et al., 2012; Miyazaki et al., 2011). Unlike SVs and chromaffin DCVs whose exocytosis is triggered by calcium binding to synaptotagmins 1, 2, and 9 (Fernández-Chacón et al., 2001; Geppert et al., 1994; Maximov and Südhof, 2005; Sørensen et al., 2003a; Xu et al., 2007), BDNF vesicles are believed to recruit calcium sensors CAPS and to be negatively regulated by Syt4, a synaptotagmin isoform that lacks calcium-binding activity in vertebrates (Dai et al., 2004; Dean et al., 2009; Sadakata et al., 2012). We found that, in spite of their remarkable differences with SVs, BDNF vesicles employ Syb2 and SNAP25 for fusion in all subcellular domains of cortical neurons. Our results imply that Syb2 and SNAP25 broadly regulate neuronal secretion and offer an alternative interpretation of previously described phenomena associated with disruption of these SNAREs in the brain. Nevertheless, release of BDNF also is controlled by SNAP47, a SNAP isoform that associates with Syb2 and SNAP25 but does not contribute to exocytosis and recycling of SVs. Cell-autonomous loss of SNAP47 impairs the layer-specific branching of callosal axons of pyramidal neurons in the somato-sensory cortex in vivo, suggesting that differentiation of cortical axons depends on autocrine BDNF/TrkB signaling rather than glutamatergic outputs onto postsynaptic targets.

RESULTS

Spatial and Temporal Dynamics of BDNF Exocytosis

To investigate the molecular mechanisms of BDNF secretion, we infected cortical neurons in primary cultures with a lentivirus encoding BDNF-pHluorin, a reporter comprised of full-length (pro) BDNF and a pH-sensitive form of GFP (Matsuda et al., 2009). The rationale for this approach and various controls that validate the appropriate post-translational modification, trafficking, and biological activity of BDNF fusion proteins are described in the accompanying Supplemental Experimental Procedures. Confirming earlier studies (Dean et al., 2012; Matsuda et al., 2009; Miyazaki et al., 2011), immunofluorescence and live time-lapse imaging showed that BDNF vesicles were scattered in processes of mature neurons; contained another secreted peptide, secretogranin2; and were largely segregated from SVs. Unlike SVs, these organelles were not anchored at synapses, and they underwent bi-directional transport in axonal and dendritic shafts (Figure 1A; Figure S1).

We then monitored the release of BDNF-pHluorin in live neurons using total internal reflection fluorescent (TIRF) time-lapse microscopy. Under these conditions, the reporter is barely detectable in intracellular vesicles due to their low lumenal pH. During exocytosis, de-acidification leads to a rapid increase in fluorescence followed by a decay due to diffusion of cargo into the extracellular medium (Figure 1B). As shown previously (Balkowiec and Katz, 2000; Matsuda et al., 2009), secretion of BDNF could be reliably induced by direct membrane depolarization with KCl, high-frequency bursts of action potentials triggered by electrical stimulation, or pharmacological augmentation of network activity with the GABA receptor blocker

picrotoxin (PTX) (Figures S2A–S2D; Movie S1). To assess the efficacy of exocytosis, we measured three parameters: (1) number of isolated fusion events that occurred during fixed time intervals (EN) (we confirmed that these events reflected release by applying a membrane-impermeable hydrophilic quencher, bromophenol blue [Harata et al., 2006]); (2) number of internal vesicles (intracellular pool [IP]) in which BDNF-pHluorin could be detected following artificial de-acidification of lumens with ammonium chloride; and (3) probability of fusion (P_f) = EN/IP ratio. This value was calculated to account for variability in the integrated area of plasma membrane and/or density of available vesicles across independent imaging sessions (Figure 1C; Figures S2E and S2F). EN and P_f were diminished when stimulation was performed in the absence of extracellular calcium or in the presence of inhibitors of calcium channels known to be required for the secretion of native BDNF (Balkowiec and Katz, 2000; Figure S2G).

SVs are clustered at presynaptic terminals where they form readily releasable pools (RRPs) adjacent to active zones. These pools are primed by SNARE complex assembly for rapid synchronous exocytosis in response to action potential-dependent calcium influx (Südhof, 2013). By contrast, side-by-side comparison of neurons carrying BDNF-pHluorin or a reporter of SVs, synaptophysin (SyP)-pHluotrin (Peng et al., 2012), indicated that secretion of BDNF is asynchronous (Figures 1D and 1E). The kinetics of BDNF release also drastically differed from transferrin receptor-positive recycling endosomes (Figures S2H–S2J). Moreover, only a fraction of BDNF vesicles fused at synapses regardless of stimulation type, as evidenced by simultaneous TIRF imaging of BDNF-pHluorin and genetically encoded pre- and postsynaptic markers, tdTomato-SV2A and EBFP2-Homer1c (Figures S2K–S2N). These results indicate that no primed vesicle pools exist that supply a synaptic or extra synaptic RRP equivalent to BDNF in cortical neurons.

Secretion of BDNF Is Directly Controlled by TeNT-Sensitive SNAREs

To explore the possibility that release of neurotransmitters and BDNF is driven by distinct SNARE complexes, we first evaluated the effects of TeNT, a protease that potently blocks the fusion of SVs by cleaving the vesicular SNARE, Syb2 (Schoch et al., 2001; Yamasaki et al., 1994). Although the extracellular application of recombinant TeNT polypeptide previously has been shown to interfere with the release of BDNF in hippocampal cultures (Matsuda et al., 2009), it is unclear if this effect was direct. Indeed, TeNT-dependent loss of glutamatergic neurotransmission (Kerschensteiner et al., 2009; Pieraut et al., 2014; Yu et al., 2004; Zhang et al., 2008) may ultimately prevent the secretion of cargo from other membrane organelles whose exocytosis is coupled with synaptic excitation (Balkowiec and Katz, 2002; de Wit et al., 2009; Dean et al., 2012). We therefore investigated the effects of genetically encoded TeNT that was expressed under the control of the synapsin promoter, either globally or in a cell-autonomous manner, in only a small fraction of synaptically connected neurons. Similar approaches were used for all subsequent analyses of individual SNAREs described below.

Quantitative immunoblotting showed a strong increase in the levels of native BDNF and BDNF-pHluorin in cultured neurons that were uniformly infected with the TeNT lentivirus (Figures 2A and 2B). We also detected an accumulation of endogenous BDNF in membrane fractions isolated from the cortices of conditional mouse mutants that harbored TeNT in glutamatergic neurons in the postnatal forebrain (Pieraut et al., 2014; Figures 2C and 2D). TIRF microscopy revealed that TeNT prevented the release of BDNF-pHluorin from cultured neurons resulting in its intra-vesicular retention during stimulation with KCl (Figures 2E and 2F). Conventional imaging of the entire vesicle pool suggested that TeNT interferes with exocytosis rather than transport from the ER to the Golgi, budding from the Golgi, and endosomal trafficking (Figures S3A–S3C).

Because release of BDNF is regulated by synaptic network activity, we next tested if TeNT-sensitive SNAREs promote the secretion in a cell-autonomous manner. To accomplish this task, BDNF-pHluorin, TeNT, and a red tracer (mCherry) were sparsely co-expressed in ~5% of cortical neurons in culture (Figures 2G and 2H; Figure S3D–S3F). Infected neurons received intact glutamatergic inputs from surrounding wild-type cells, as demonstrated by GCaMP-based imaging of calcium signals elicited by the application of PTX (Figure 2I; Figures S3G and S3H). These experimental settings allowed us to bypass the effects of the protease on exocytosis of SVs and to monitor the fusion of BDNF vesicles in distinct subcellular domains of single neurons (Movies S2 and S3). TeNT abolished secretion in this case as well, even when cultures were depolarized continuously. Remarkably, quantifications of EN and P_f demonstrated that exocytosis was uniformly and nearly completely blocked in cell bodies, dendrites, and axons (Figures 2J–2L).

Exocytosis of BDNF Is Driven by the Vesicular SNARE Syb2

At least nine genes encoding vesicular SNAREs are expressed in the mammalian brain, including seven different Syb/VAMPs, YKT6, and Sec22b (Figure 3A, based on Allen Brain Atlas database). We systematically examined the sensitivity of these SNAREs to TeNT by immunoblotting following the overexpression of cDNAs in HEK293 cells. Confirming earlier experiments with Sybs/VAMPs 1–3 (McMahon et al., 1993; Yamasaki et al., 1994), these proteins were cleaved in the presence of the protease whereas the remaining isoforms were resistant (Figure 3B). We then designed small hairpin RNAs (shRNAs) that disrupt the expression of native TeNT-sensitive Syb/VAMPs, and we studied the outcomes of knockdowns (KDs) on neuronal secretion of BDNF using a combination of biochemical and TIRF imaging readouts. We initially introduced pairs of lentiviruses driving hairpins under the control of H1 promoter to target two non-overlapping coding regions of each Syb/VAMP transcript. Single shRNAs from a mix that produces a phenotype were then tested in isolation or co-expressed with the rescue shRNA-resistant cDNA from a dual H1/Synapsin-promoter lentivirus vector (Figure S4A; Table S1). The potencies and specificities of these hairpins were confirmed by immunohistochemistry and immunoblotting with relevant antibodies (Figures S4D–S4F; data not shown).

Loss of Syb2 alone fully recapitulated the effects of TeNT. KD of this SNARE in all neurons in culture resulted in an

Please cite this article in press as: Shimojo et al., SNAREs Controlling Vesicular Release of BDNF and Development of Callosal Axons, Cell Reports (2015), http://dx.doi.org/10.1016/j.celrep.2015.04.032

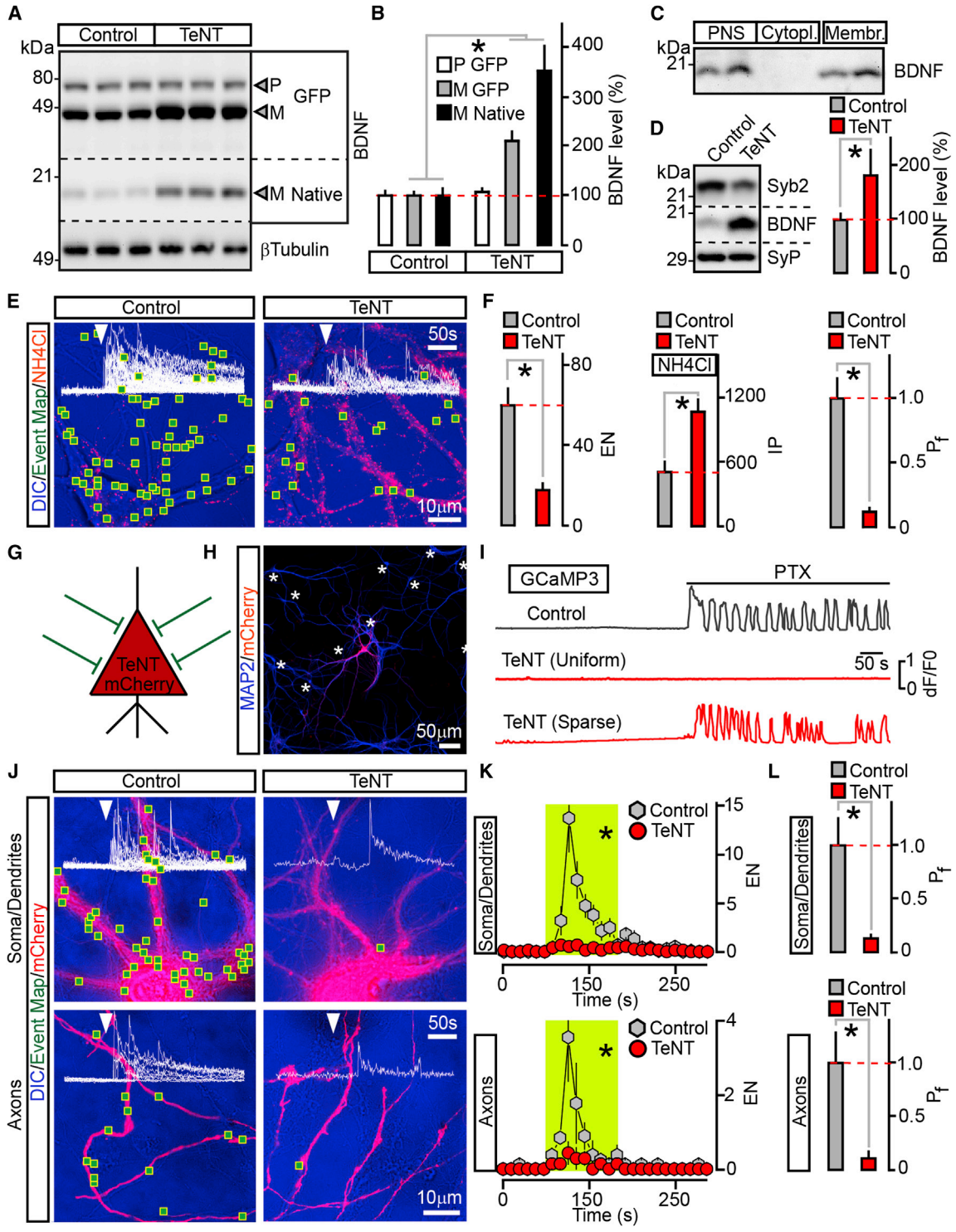

Figure 2. Analysis of BDNF Release in Neurons Carrying TeNT

(A and B) Measurements of pro (P) and mature (M) BDNF levels in cultured neurons that uniformly expressed BDNF-pHluorin alone (Control) or with TeNT. Quantitative immunoblotting was performed with an antibody to BDNF that recognizes all native and recombinant forms. βTubulin was used as a loading standard. Representative blots and averaged values from three experiments are shown.

(C) Subcellular fractions of mouse forebrains were isolated by differential centrifugation and probed by immunoblotting for native BDNF. PNS, post-nuclear supernatant.

(legend continued on next page)

accumulation of mature BDNF forms and inhibited the depolarization-dependent exocytosis of BDNF-pHluorin without altering the subcellular localization of intracellular vesicles. In contrast, KDs of two other TeNT substrates, Syb1 and Syb3, failed to significantly affect the BDNF levels, EN, and P_f (Figures 3C–3F; Figures S3C, S4B, and S4C). TIRF imaging of BDNF-pHlorin in sparsely infected cultures demonstrated that, similar to TeNT, KD of Syb2 blocks the exocytosis in a cell-autonomous manner and in all subcellular domains. Single mCherry-tagged neurons carrying a Syb2-directed shRNA had a strong reduction of both the frequency of evoked fusion events and P_f across somas, dendrites, and axons, despite receiving excitatory inputs from wild-type cells. These defects were rescued by the Syb2 cDNA containing silent mutations in the shRNA target site, hence ruling out off-target artifacts (Figures 3G–3I; Figure S4G). Also, native Syb2 could be detected in a significant fraction of BDNF vesicles by immunofluorescence microscopy, indicating that these organelles recruit Syb2 (Figures S4H–S4J).

Secretion of BDNF Is Regulated by Two Membrane SNAPs

Our results imply that Syb2 directly promotes the release of BDNF independently of its presynaptic function and, surprisingly, does so in axons, dendrites, and somas. To test if this previously unappreciated function of Syb2 involves interactions with unique vesicle-specific effectors on the plasma membrane, we focused on members of the membrane SNAP protein family with abundant expression in the brain, SNAPs 23, 25, 29, and 47 (Figure 4A; based on Allen Brain Atlas database; Holt et al., 2006; Johansson et al., 2008; Su et al., 2001; Suh et al., 2010). Imaging of cortical cultures that broadly expressed SNAP-specific hairpins demonstrated that exocytosis of BDNF-pHluorin was suppressed after the ablation of SNAP25 and SNAP47 (Figures 4B–4D). However, only KD of SNAP25 resulted in an accumulation of bulk intracellular BDNF under these conditions, indirectly suggesting that SNAP47 has a modulatory and/or spatially restricted function (Figures S5A and S5B).

Previous in vitro studies have shown that SNAP47 is unable to fully substitute for SNAP25 in fusion of liposomes driven by SNARE complexes containing Syb2 and Syntaxin1 (Holt et al., 2006). SNAP47 also has been implicated in hippocampal long-term potentiation (LTP) (Jurado et al., 2013), yet its role in secretion has remained unclear. The involvement of SNAP47 in exocytosis of BDNF vesicles is intriguing, since induction of Hebbian plasticity critically depends on BDNF signaling (Kang and Schuman, 1995; Park and Poo, 2013; Patterson et al., 1996). To gain more insight into functions of two SNAP isoforms in BDNF trafficking, we examined the cell-autonomous outcomes of their KDs on exocytosis of BDNF-pHluorin in single sparsely infected neurons. KD of SNAP25 uniformly abolished the depolarization-induced release in all subcellular domains. On the contrary, SNAP47-deficient cells only exhibited a prominent loss of exocytosis in axons, albeit we also detected a shift in kinetics of vesicle fusion across their entire surface (Figures 4E–4J; Figure S6). Consistent with these notions, both SNAP isoforms were distributed throughout neuronal processes (Figures S5F–S5H). The phenotypes associated with each KD could be reversed by corresponding shRNA-insensitive cDNAs (Figures 4E–4J; Figures S5A–S5E and S6). Neither KD altered the distribution of internal BDNF vesicles, making it unlikely that secretion was disrupted due to abnormal intracellular trafficking (Figure S3C). To test whether SNAP47 and SNAP25 interact with each other, we immunoprecipitated these SNAREs with isoform-specific antibodies from mouse brain extracts. Immunoblotting showed that SNAP47 and SNAP25 are abundant in complexes that contain Syb2 and syntaxin1 (Figure 4K).

To mimic activity-dependent secretion using a more physiologically relevant paradigm, we also induced exocytosis with bursts of action potentials. Cortical cultures were sparsely infected with BDNF-pHluorin and mCherry, and axonal secretion was monitored before, during, and after 30-s stimulus trains that were triggered at various frequencies by brief injection of current through an extracellular electrode. Fusion events were detectable, yet, relatively rare at 10 Hz, whereas 100-Hz trains elicited robust responses. Nevertheless, TeNT or KD of SNAP47 potently suppressed EN and P_f at both frequencies (Figures 5A–5D).

SNAP47-Deficient Neurons Have Normal Exocytosis and Recycling of SVs

Our experiments reveal largely promiscuous roles of Syb2 and SNAP25 in membrane fusion and identify SNAP47 as a critical

(D) Quantitative immunoblot measurements of mature BDNF levels in membrane fractions prepared from cortices of wild-type P15 mice (Control) and their littermates carrying TeNT in glutamatergic neurons (*CamKII*α:Cre/*R26*^{floxstopTeNT}) (n = 5 mice/genotype). The reduction of Syb2 band intensity is due to cleavage by TeNT, which makes Syb2 undetectable with antibodies.

(E and F) TIRF microscopy analysis of vesicle exocytosis in DIV15 cultured neurons that globally expressed BDNF-pHluorin without or with TeNT. (E) Pseudo-colored differential interference contrast (DIC) images with superimposed maps of all sites where vesicle fusion was detected during transient depolarization with KCl (2 min). Red puncta are intracellular reporter-positive vesicles visualized by perfusing 50 mM NH_4Cl following stimulation. (F) Averaged EN (calculated for a 2-min window of stimulation in entire fields of view), IP, and P_f (n = 9/group).

(G–L) Cell-autonomous effects of TeNT on BDNF release. Neurons were sparsely infected (~5% of the total population) with lentiviruses encoding BDNF-pHluorin and mCherry alone or together with TeNT. These cells received synaptic inputs from wild-type neurons, as depicted in (G). (H) An example of infection pattern is shown. Cultures were stained for MAP2. Asterisks label somas of reporter-negative cells. (I) PTX-induced (100 μM) calcium signals were recorded from neurons co-expressing TeNT, mCherry, and GCaMP3, either globally or sparsely, as described above. (J–L) Exocytosis of BDNF vesicles was monitored by TIRF microscopy at DIV15. (J) DIC and mCherry images show mapped regions of somato-dendritic and axonal domains where vesicle fusion was observed during 2-min depolarization with KCl. Superimposed traces of BDNF-pHluorin fluorescence sampled in time-lapse mode (inserts, arrows mark times of excitation) reflect exocytosis in each site. (K) Averaged EN in different subcellular compartments of individual neurons, plotted as a function of time (10-s bin). Green boxes mark the window of transient excitation. (L) Mean P_f of evoked fusion in somas, dendrites, and axons (n = 7–8/group).

Quantifications are represented as mean ± SEM; n corresponds to numbers of trials performed with at least three independent culture preparations; *$p < 0.001$ (Student's t test).

Please cite this article in press as: Shimojo et al., SNAREs Controlling Vesicular Release of BDNF and Development of Callosal Axons, Cell Reports (2015), http://dx.doi.org/10.1016/j.celrep.2015.04.032

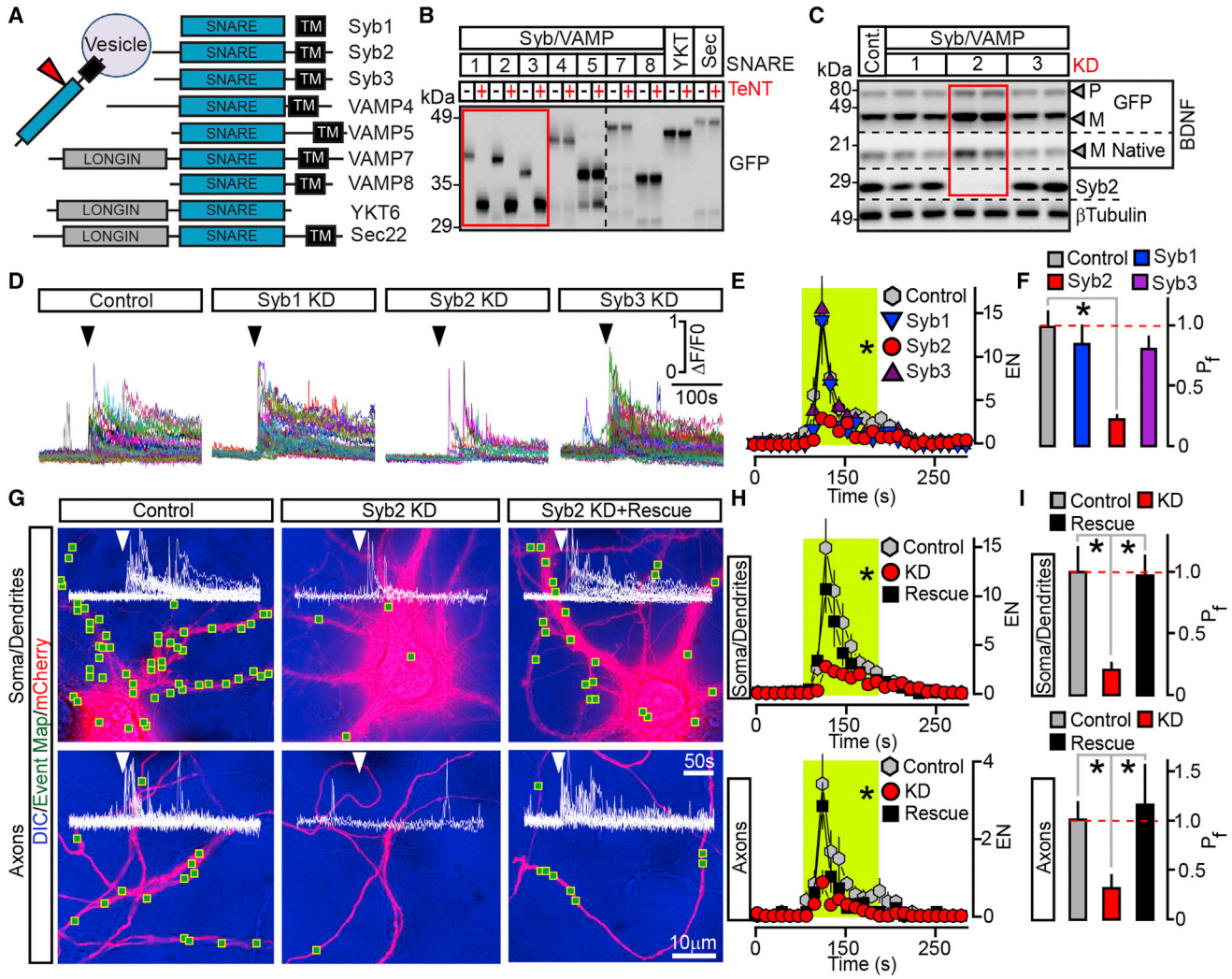

Figure 3. Syb2 Drives the Exocytosis of BDNF Vesicles in Axons and Dendrites Independently from Its Presynaptic Function

(A) Domain structures of vesicular SNAREs.

(B) Biochemical assessment of SNARE sensitivity to TeNT. Homogenates of HEK293 cells expressing different GFP-tagged SNAREs alone or together with TeNT were probed by immunoblotting for GFP. Dashed line indicates splicing of two different gels.

(C–F) Cortical cultures were broadly co-infected at DIV5 with lentiviruses expressing BDNF-pHluorin and two shRNAs that target non-overlapping sequences of specific TeNT-sensitive Syb/VAMPs (KD). All experiments were performed at DIV15. (C) Immunoblot analysis of pro- (P) and mature (M) BDNF levels was performed using antibodies to BDNF and βTubulin, as a loading standard (n = 6 control and Syb/VAMP-deficient cultures, examined in duplicates). Quantifications are shown in Figure S4B. (D) TIRF traces represent all events of depolarization-induced vesicle fusion detected in isolated sites of control and Syb1–3-deficient neurons. Arrows mark times of excitation. (E) Averaged EN, plotted as a function of time. Green box marks the window of transient excitation. (F) Mean P_f across the cell bodies and processes is shown. Control, n = 7; Syb1 KD, n = 6; Syb2 KD, n = 7; Syb3 KD, n = 7; *p < 0.05 (ANOVA).

(G–I) Syb2 directly mediates BDNF release in all subcellular domains. Exocytosis was monitored by TIRF microscopy in somas, dendrites, and axons of isolated neurons in DIV15 cultures that were sparsely co-infected with viruses encoding BDNF-pHluorin, mCherry, and Syb2 shRNA without or with shRNA-resistant rescue cDNA. (G) DIC and mCherry images show mapped regions of somato-dendritic and axonal domains where fusion was observed during transient depolarization. Superimposed traces of BDNF-pHluorin fluorescence reflect exocytosis in each site. (H) Averaged EN in different subcellular compartments, plotted as a function of time. (I) Mean P_f in somas, dendrites, and axons (n = 11–14/group). *p < 0.01 (ANOVA). See also Figure S4.

Data are plotted as mean ± SEM.

regulator of vesicular release. To test if SNAP47 is necessary for exocytosis of SVs, we examined synapses of mature neurons in culture by confocal microscopy and electrophysiology. Uniform expression of TeNT or KD of Syb2, SNAP25, or SNAP47 did not disrupt the formation of glutamatergic and GABAergic terminals, consistent with previous notions that vesicular exocytosis is not necessary for gross synaptic differentiation in vitro (Harms and Craig, 2005; Schoch et al., 2001; Figure S7; data not shown). We then performed whole-cell recordings to evaluate the properties of different synapse types. As expected, TeNT and

hairpins against Syb2 and SNAP25 diminished the amplitudes of evoked excitatory and inhibitory postsynaptic currents (eEPSCs and eIPSCs, respectively) and the rates of spontaneous SV fusion alike. However, synaptic strength was unaltered in neurons lacking SNAP47, despite their defects in exocytosis of BDNF (Figures 5E–5H; Table S2). In addition, wild-type and SNAP47-deficient neurons had indistinguishable profiles of PSC depression and de-synchronization during action potential trains as well as kinetics of quantal AMPA- and GABA-type currents (Figures 5I–5L; Table S2; data not shown). Hence, unlike Syb2 and SNAP25, SNAP47 appears to be unnecessary for SV exocytosis and recycling.

SNAP47 Is Essential for Axon Differentiation In Vitro and In Vivo

Targeted disruption of vesicular release in animal brains is becoming increasingly popular for studies of the role of neuronal activity in regulation of connectivity. For instance, several laboratories have shown that inducible expression of genetically encoded TeNT interferes with wiring of olfactory sensory neurons, photoreceptors, pyramidal neurons, and inhibitory GABAergic interneurons in the cerebral cortex and hippocampus (Kerschensteiner et al., 2009; Pieraut et al., 2014; Wang et al., 2007; Yu et al., 2004). While these phenomena are widely believed to reflect the instructive role of excitatory synaptic outputs, the involvement of BDNF or other secreted peptides cannot be ruled out. Indeed, BDNF is known to be necessary for axon growth and branching (Cao et al., 2007; Cheng et al., 2011; Marshak et al., 2007; Park and Poo, 2013), and we found that, by cleaving Syb2, TeNT directly blocks the release of fast neurotransmitters and BDNF. Notably, Syb2, SNAP25, and SNAP47 are expressed in the developing brain prior to the onset of synaptogenesis, with SNAP47 turning on as early as embryonic day 10 (Holt et al., 2006). We therefore monitored secretion of BDNF in axons of differentiating SNAP47-deficient cortical neurons, and we examined axon morphologies in culture and in the mouse brain in vivo. As demonstrated above, this strategy enabled us to interfere with axonal exocytosis of BDNF without affecting SVs. We initially imaged BDNF-pHluorin in isolated mCherry-tagged neurons in dissociated cultures. These cells were sparsely infected with viruses immediately after plating and analyzed 6 days later, when a marker of presynaptic boutons, synapsin1, remained diffusely distributed in axons. Immunostaining confirmed that endogenous SNAP47 and other SNAREs were present in axons at this stage (Figures S8A and S8B). Differentiating neurons displayed robust exocytosis of BDNF-pHluorin during membrane depolarization (Figures 6A–6C; Movie S4). Secretion was blocked by TeNT or KD of SNAP47, but was restored in the presence of rescue SNAP47 cDNA (Figures 6D–6H).

To determine how axonal exocytosis of BDNF impacts axon differentiation, a mix of two plasmids encoding a monomeric form of Venus and shRNA directed against SNAP47 was unilaterally introduced into the somatosensory cortex of E15.5 mouse embryos via electroporation (Courchet et al., 2013). This method allows for selective targeting of callosally projecting pyramidal neurons that populate the superficial layers 2/3. As the first step, the outcomes of SNAP47 KD in layer 2/3 neurons on their axon morphologies were assessed in cultures prepared from the cortices of electroporated embryos. SNAP47-deficient neurons (~1% of the entire pool, as determined by mVenus imaging, data not shown) had a slightly increased total axon length, but exhibited a significant reduction in the number of terminal branches. The branching defect could be reversed with shRNA-resistant SNAP47 cDNA or by continuous incubation with recombinant BDNF added in the culture medium (Figures 7A and 7B).

We then investigated the SNAP47 function in vivo, by imaging coronal cortical sections from mice that were electroporated at E15.5 and sacrificed at postnatal day 21 (P21). At P21, axons establish adult-like patterns of innervation in layers 2/3 and 5, both ipsi- and contralaterally (Courchet et al., 2013). On the contralateral side, the genetic manipulation was axon specific since neurons projected into the normal environment. Immunolabeling of sections isolated from wild-type animals showed that native SNAP47 was abundant in callosal axons (Figure S8C). Axons of mVenus-positive SNAP47-deficient neurons formed, grew, and successfully crossed the midline, but had a drastically reduced terminal arborization in the contralateral layers 2/3. Again, the defect of terminal branching was alleviated by co-expression of SNAP47 shRNA with shRNA-insensitive cDNA (Figures 7C and 7D). Nonetheless, KD of SNAP47 had no detectable effect on density of dendritic spines (Figures S8D and S8E), indicating that disruption of connectivity was likely restricted to axons. To ensure that these changes in callosal axon structure are attributable to abnormal BDNF signaling, we performed in utero electroporation with shRNAs against BDNF, or its receptor, TrkB. The morphological defects of contralateral axons of BDNF- and TrkB-deficient layer 2/3 neurons were similar to SNAP47-deficient neurons, albeit KD of BDNF produced a more robust effect with significant attenuation of branching in layer 5 (Figures 7C and 7D; Figures S8F and S8G).

DISCUSSION

In summary, these studies elucidate the roles of SNAREs in vesicular exocytosis, BDNF secretion, and neural circuit development. A large body of work shows that Syb2 and SNAP25 are essential for calcium-induced release of neurotransmitters and monoamines in central neurons and chromaffin cells, respectively (Sørensen et al., 2003b; Südhof, 2013; Südhof and Rothman, 2009). These SNAREs are thought to operate by priming vesicles and catalyzing fusion at specific sites, such as the presynaptic active zones. Remarkably, Syb2 and SNAP25 also trigger the release of BDNF from organelles that traffic and fuse with the plasma membrane across axons and dendrites, and do not form discrete pools that are primed for rapid exocytosis. By contrast, SNAP47 plays a more restricted role, perhaps as a part of a unique SNARE complex. SNAP47 interacts with SNAP25, promotes the exocytosis of BDNF in a cell-autonomous manner, but appears to be dispensable for synaptic release from SVs. Thus, two distinct types of neuronal vesicles share Syb2 and SNAP25, but their exocytosis is differentially controlled through combinatorial use of SNAPs.

Experiments with mutant animals carrying TeNT have led to a hypothesis that experience-driven refinement of connectivity is guided by neurotransmission between two relaying neurons in a given circuit (Okawa et al., 2014). Our findings challenge the

Please cite this article in press as: Shimojo et al., SNAREs Controlling Vesicular Release of BDNF and Development of Callosal Axons, Cell Reports (2015), http://dx.doi.org/10.1016/j.celrep.2015.04.032

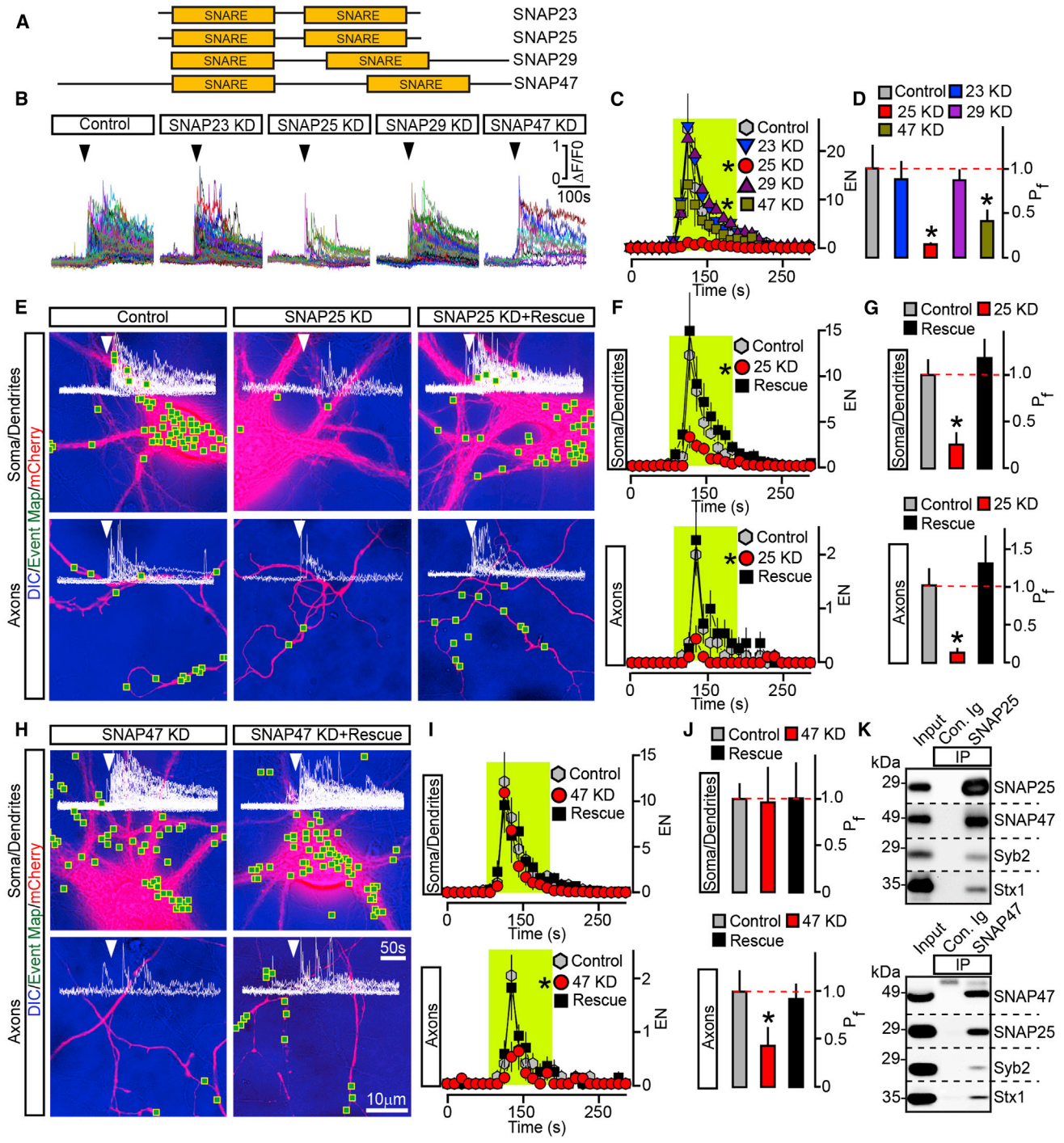

Figure 4. Exocytosis of BDNF Vesicles Is Controlled by Two Different SNAPs

(A) Domain structures of vertebrate SNAREs of the SNAP family.

(B–D) Outcomes of global ablation of SNAPs on BDNF release. Cortical cultures were co-infected at DIV5 with viruses expressing BDNF-pHluorin and two shRNAs that target non-overlapping sequences of specific SNAP isoforms (KD). Exocytosis was monitored at DIV15 by TIRF imaging. (B) Sample traces reflect all fusion evens in control and SNAP-deficient neurons. Arrows mark times of depolarization with KCl. (C) Averaged EN, plotted as a function of time. (D) Mean P_f across neuronal somas and processes. Control, n = 10; SNAP23 KD, n = 8; SNAP25 KD, n = 8; SNAP29 KD, n = 7; SNAP47 KD, n = 8; *$p < 0.01$ and < 0.05 for SNAP25 and SNAP47, respectively (ANOVA).

(E–J) Cell-autonomous effects of SNAP ablation on BDNF release. Exocytosis was monitored by TIRF microscopy in isolated neurons in DIV15 cultures that were sparsely co-infected with viruses encoding BDNF-pHluorin, mCherry, and shRNAs against indicated SNAPs without or with corresponding rescue cDNAs.

(legend continued on next page)

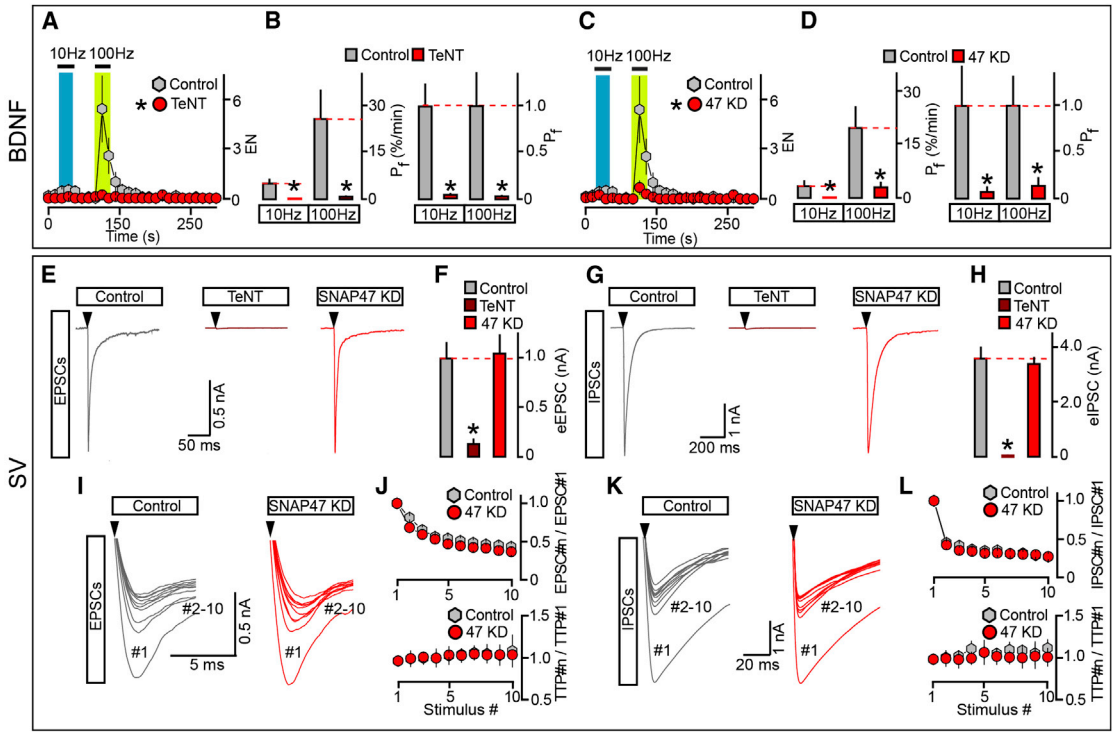

Figure 5. SNAP47 Promotes the Exocytosis of BDNF but Not Neurotransmitter Vesicles

(A–D) Frequency dependence of BDNF release in isolated wild-type and SNARE-deficient neurons. Cultures were sparsely infected with BDNF-pHluorin and mCherry lentiviruses alone or together with TeNT or shRNA against SNAP47 (KD). TIRF imaging was performed at DIV15. Exocytosis was elicited by electrical stimulation at 10 and 100 Hz (1 ms/10V/pulse) and monitored in mCherry-tagged axons. Each stimulus train was applied for 30 s. (A and B) Averaged EN and P_f. Colored boxes mark the times of action potential trains. P_f values are shown without normalization or as a fraction of control. Control, n = 14; TeNT, n = 10; *p < 0.001 (Student's t test). (C and D) EN and P_f were measured in control and SNAP47-deficient neurons and represented as described above. EN: Control, n = 14, this group is the same as for TeNT experiments; SNAP47 KD, n = 16. P_f: Control, n = 16; SNAP47 KD, n = 19. *p < 0.001 (ANOVA).

(E–L) Exocytosis of SVs in neurons carrying TeNT or shRNA against SNAP47. Cortical cultures were uniformly infected with corresponding lentiviruses. The eEPSCs and eIPSCs were sampled at DIV15 in whole-cell voltage clamp mode. The eEPSCs and eIPSCs were triggered by single-action potentials or 10-Hz stimulus trains, and were pharmacologically isolated by the addition of GABA or AMPA/NMDA receptor blockers. (E and F) Samples of individual eEPSCs (E) (scale bars apply to all traces and arrows mark times of action potentials) and averaged eEPSC amplitudes (F). Control, n = 13; TeNT, n = 11; SNAP47 KD, n = 13. *p < 0.001 (ANOVA). (G and H) Samples of single eIPSCs (G) and averaged eIPSC amplitudes (H). Control, n = 19; TeNT, n = 3; SNAP47 KD, n = 14. *p < 0.001 (ANOVA). (I–L) Short-term plasticity of excitatory and inhibitory synapses in wild-type and SNAP47-deficient neurons. (I and K) Onsets of aligned EPSCs (I) and IPSCs (K) that were elicited by 10-Hz trains of ten action potentials (arrows). (J and L) (Top) Averaged profiles of synchronous EPSC (J) and IPSC (L) depression during repetitive stimulation are presented as ratios of PSC amplitudes. (Bottom) Averaged profiles of EPSC (J) and IPSC (L) de-synchronization are plotted as ratios to times to peak (TTP). EPSCs: Control, n = 12; SNAP47 KD, n = 8. IPSCs: Control, n = 16; SNAP47 KD, n = 12.

Data are plotted as mean ± SEM. See also Figure S7 and Table S2.

generality of this model and underscore an alternative pathway that depends on autocrine BDNF/TrkB signaling. First, we show unambiguously that, by cleaving Syb2, TeNT abolishes the release of neurotransmitters and BDNF. We further demonstrate that cell-autonomous ablation of SNAP47, which evidently does not affect SVs, leads to defects in layer-specific branching of callosal axons that are similar to those caused by KD of BDNF or its receptor, TrkB, and those previously detected upon expression of TeNT in pyramidal neurons in the same cortical area (Wang et al., 2007). Neurotransmitters and peptides may impact axon and synapse development by binding to their receptors in spatially segregated micro-domains. Our

Aligned DIC and mCherry images show mapped sites of depolarization-induced fusion, actual events of exocytosis in each site, EN plotted as a function of time, and P_f (n = 9–11/group). (E–G) Examples of exocytosis, averaged EN, and P_f in different subcellular compartments of control and SNAP25-deficient neurons are shown. *p < 0.01 (ANOVA). (H–J) Examples of exocytosis, mean EN, and P_f in SNAP47-deficient neurons. *p < 0.05 (ANOVA). Control groups apply to both SNAP isoforms. Quantifications are represented as mean ± SEM. See also Figures S5 and S6.

(K) Solubilized proteins were co-immunoprecipitated (IP) from mouse forebrain extracts with control antibody (Ig) or antibodies against SNAP25 (top) or SNAP47 (bottom). Attached complexes were examined by immunoblotting with antibodies to SNAP25, SNAP47, Syb2, and Syntaxin1. Equal amounts of total protein were applied to each lane.

Please cite this article in press as: Shimojo et al., SNAREs Controlling Vesicular Release of BDNF and Development of Callosal Axons, Cell Reports (2015), http://dx.doi.org/10.1016/j.celrep.2015.04.032

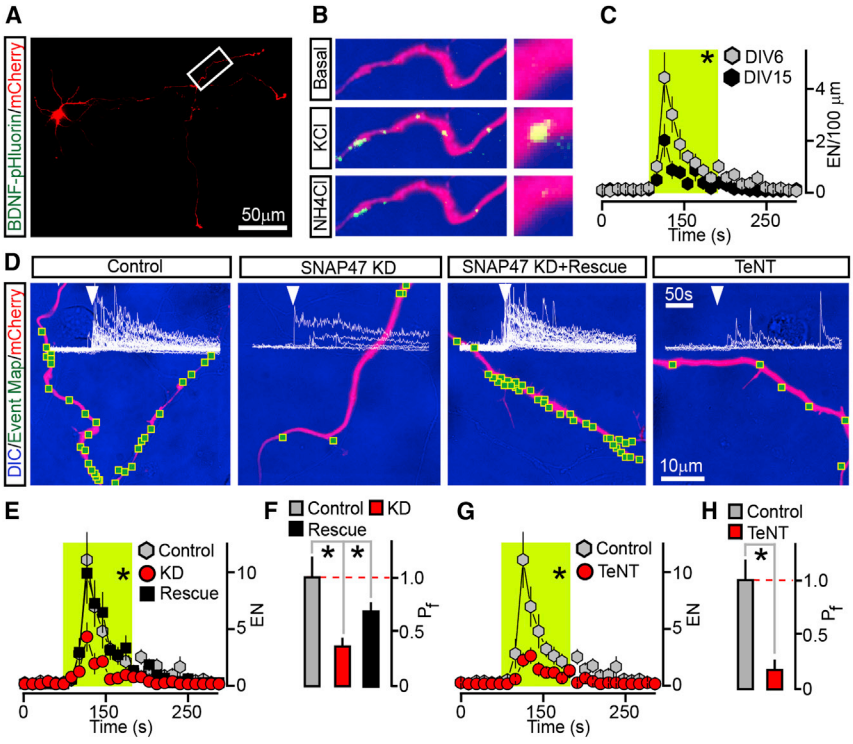

Figure 6. Analysis of BDNF Release in Differentiating Axons

Cultured cortical neurons were sparsely co-infected at DIV0 with BDNF-pHluorin and mCherry lentiviruses alone (Control) or together with viruses encoding TeNT or shRNA against SNAP47 (without or with rescue cDNA). Axonal exocytosis was monitored by TIRF microscopy at DIV6.

(A) Typical low-magnification image shows axons of a neuron tagged with mCherry.

(B) Examples of BDNF-pHluorin fluorescence in a distal fragment of an axon under the normal conditions (Basal) during depolarization with KCl and after vesicle de-acidification with NH_4Cl.

(C) Averaged EN in axons of mature (DIV15) and differentiating (DIV6) wild-type neurons were normalized to axon length and plotted as a function of time. DIV6, n = 10; DIV15, n = 7.

(D) DIC and mCherry images show mapped sites of depolarization-induced fusion and actual BDNF-pHluorin responses detected in each site of control, SNAP47-deficient, and TeNT-expressing neurons.

(E–H) Averaged EN and P_f. *p < 0.02 (ANOVA). Note that, in this case, rescue is significant but incomplete, perhaps due to the short time course of cDNA overexpression.

See also Figures S8A and S8B.

results favor the scenario that axonally released BDNF promotes cortical axon branching via TrkB receptors localized on the same axon (Cao et al., 2007; Cheng et al., 2011).

Peptidergic vesicles contain diffusible cues other than BDNF (Lessmann et al., 2003), though their cargo may vary in different neuron classes and developmental stages. Identification of SNAREs essential for BDNF exocytosis will facilitate the further understanding of mechanisms of peptide secretion and will enable the design of new genetic tools to investigate the outcomes of secretion on neural circuit structure and information processing. In this regard, SNAP47 is a particularly attractive molecule due to its selectivity and unusually large size with putative sequences that may mediate protein-protein interactions (Holt et al., 2006). It would be of great interest to explore the interplay between this SNARE and other known and yet unidentified elements of membrane-trafficking machinery, including calcium sensors (Sadakata et al., 2012; Südhof, 2013) and scaffolds that may recruit organelles to release sites.

EXPERIMENTAL PROCEDURES

Neuronal Cultures

Cortices of P1 pups were dissociated by trypsin digestion; cells were plated on circle glass coverslips (Harvard Apparatus) coated with poly-D-Lysine (Sigma-Aldrich). Cultures were maintained for 4 days in MEM (Invitrogen) supplemented with fetal bovine serum (FBS), B-27 (Invitrogen), glucose, transferrin, and Ara-C (Sigma) followed by incubation in the serum-free medium. Neurons were seeded at 25,000–50,000 cells/cm^2 for imaging and electrophysiological studies and at 150,000–175,000 cells/cm^2 for immunoblotting. In both preparations, the densities of astrocytes did not exceed 2%–3%, as determined by immunostaining for GFAP.

Virus Infection

Recombinant lentiviruses were produced by co-transfection of HEK 293T cells with corresponding shuttle vectors and pVSVg and pCMVΔ8.9 plasmids that encode the elements essential for packaging viral particles. Transfections were performed using the FuGENE reagent (Promega). Secreted viruses were harvested 48 hr later and cleared by brief centrifugation. For uniform expression of fluorescent reporters and shRNA/rescue constructs, cultures were infected at 5 days in vitro (DIV5) with 100 μl viral supernatants per 1 ml of medium. This protocol was optimized to achieve >95% infection efficiency. For sparse infection, dissociated neurons were seeded onto Matrigel- (BD Biosciences) coated 12-well plates and treated with viruses immediately after plating. Then 24 hr after infections, cells were washed three times with PBS, dissociated with trypsin, and mixed with non-infected neurons at a 1:20 ratio.

Immunocytochemistry

Neurons attached to the glass coverslips were rinsed once in PBS, fixed on ice in 4% paraformaldehyde (PFA) and 4% sucrose in PBS, and permeabilized for 5 min at room temperature in 0.2% Triton X-100 (Roche). Permeabilized neurons were incubated for 30 min in blocking solution containing 5% BSA (Sigma, fraction V) and 5% normal donkey serum, followed by an overnight incubation with primary and corresponding fluorescently labeled secondary antibodies diluted in the same solution. The coverslips were mounted on glass slides with Aqua-Poly/Mount medium (Polysciences). Images were collected under a Nikon C2 confocal microscope using 10× (numerical aperture [N.A.] 0.45), 20× (N.A. 0.75), and 60× (N.A. 1.40) PlanApo objectives. Digital images were analyzed with the Nikon Elements software package. Digital manipulations were equally applied to all pixels. Analyses of organelle co-localization were performed with NIH ImageJ software.

Immunoprecipitations

Cortices of wild-type mice were homogenized in 20 mM HEPES-NaOH (pH 7.4), 320 mM sucrose, 5 μg/ml leupeptin, 2 μg/ml aprotinin, and 1 μg/ml pepstatin. Membrane fractions were isolated by two sequential steps of centrifugation at 3,000 and 100,000 × *g* and solubilized for 1 hr in 20 mM HEPES-NaOH (pH 7.4), 150 mM NaCl, and 1% Triton X-100. Protein extracts

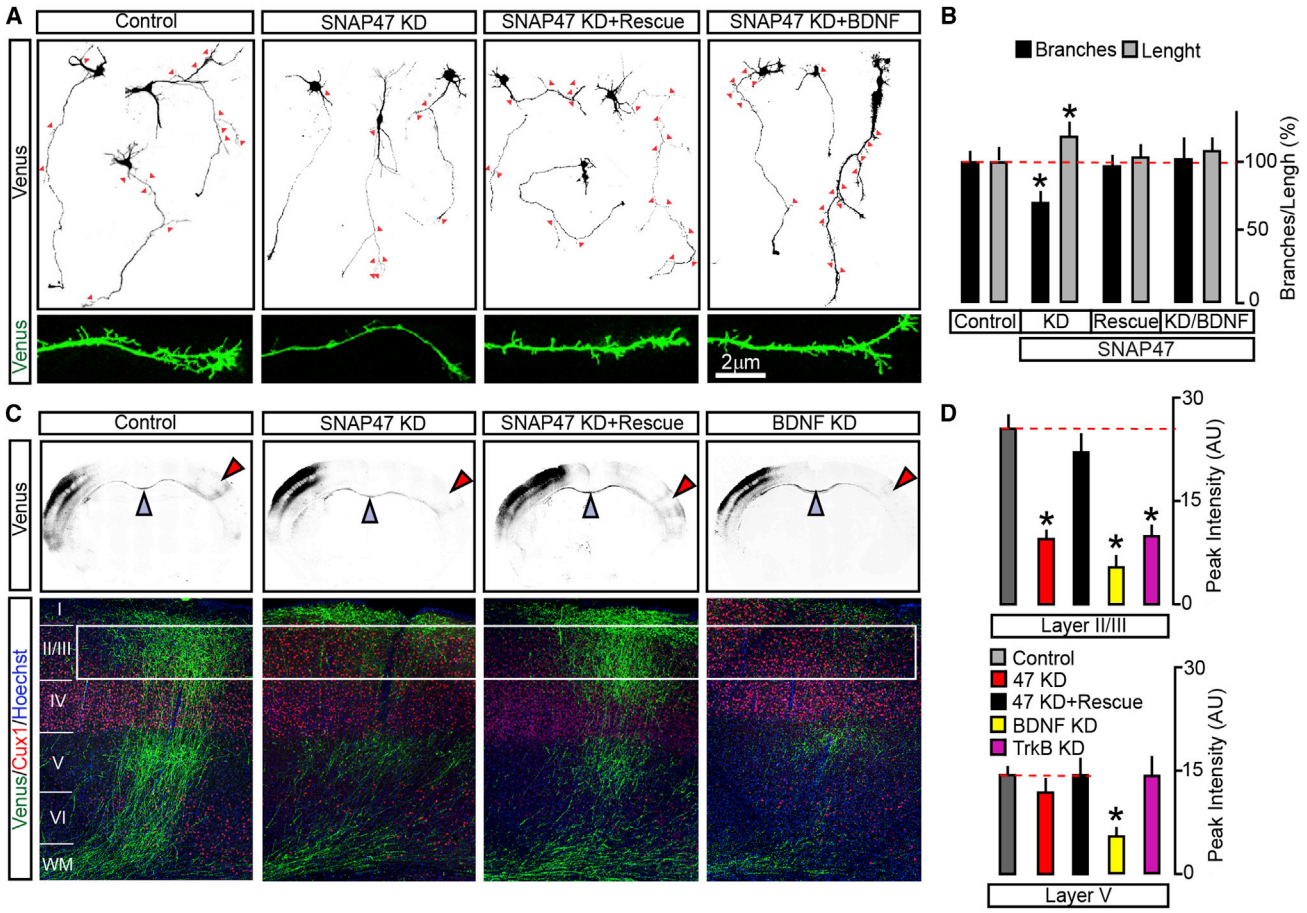

Figure 7. SNAP47 Is Essential for BDNF-Dependent Axon Branching In Vitro and In Vivo

(A and B) Cortices of E15.5 mouse embryos were electroporated ex vivo with the pSCV2-mVenus plasmid together with control shuttle vector or vectors driving the expression of SNAP47 shRNA alone or with rescue cDNA. Morphologies of differentiating mVenus-positive axons were then examined in primary cultures prepared from these mice. Axon identities were confirmed by immunostaining for SMI312 and MAP2 (not shown). (A) Typical images of DIV5 neurons carrying indicated constructs. Cultures were maintained in the normal medium or with the addition of recombinant BDNF (50 ng/ml, applied at DIV1). Arrows mark each axonal branch. (Bottom) Enlarged fragments of axons. (B) Quantifications show total axon length and branch numbers. Data from three independent cultures were normalized to control in each case. Control, n = 62 axons; SNAP47 KD, n = 74; SNAP47 KD + Rescue, n = 51; SNAP47 KD + BDNF, n = 14. *$p < 0.05$ (ANOVA).

(C and D) E15.5 embryos were in utero electroporated into one cortical hemisphere with mVenus tracer together with control shuttle vector or vectors encoding indicated shRNAs. Axon branching was examined by imaging of brain slices at P21. (C) (Top) Low-magnification images of coronal brain sections. mVenus signal is shown in black. Electroporated (ipsilateral) sides are on the left. Blue arrows mark corpus callosum. Red arrows point to contralateral branching. (Bottom) Confocal images of contralateral sides of cortical sections stained for mVenus, a layer-specific marker (Cux1), and a nuclear marker (Hoechst). (D) Average surface areas of mVenus fluorescence in layers 2/3 and 5 of contralateral cortex. Control, n = 11 mice; SNAP47 KD, n = 8 mice; SNAP47 KD + Rescue, n = 5 mice; BDNF KD, n = 3 mice; TrkB KD, n = 8 mice. *$p < 0.001$ (ANOVA).

Data are plotted as mean ± SEM. See also Figure S8.

were cleared by centrifugation at 100,000 × *g* and incubated overnight with sepharose beads (Sigma) coated with anti-SNAP25, anti-SNAP47, or control antibodies. Attached complexes were then washed five times with extraction buffer, eluted from the beads with an SDS gel loading buffer, and used for immunoblotting.

Electrophysiology

Evoked synaptic release was triggered by 1-ms current injections with a local extracellular stimulating electrode (FHC). Postsynaptic currents were monitored in whole-cell mode from randomly selected nearby neurons using a Multiclamp 700B amplifier (Axon Instruments). The frequency, duration, and magnitude of extracellular stimuli were controlled with Model 2100 Isolated Pulse Stimulator (A-M Systems). The whole-cell pipette solution contained 135 mM $CsCl_2$, 10 mM HEPES-NaOH (pH 7.4), 1 mM EGTA, 1 mM Na-ATP, 0.4 mM Na-GTP, and 1 mM QX-314. The resistance of filled pipettes varied between 3 and 5 mOhm. The bath solution contained 140 mM NaCl, 5 mM KCl, 2 mM $CaCl_2$, 0.8 mM $MgCl_2$, 10 mM HEPES-NaOH (pH 7.4), and 10 mM glucose. EPSCs and IPSCs were separated pharmacologically by the addition of picrotoxin (100 μM) or APV (50 μM) and CNQX (10 μM), respectively, to the bath solution. Spontaneous EPSCs and IPSCs were monitored under the same conditions but in the presence of tetrodotoxin (1 μM). The currents were sampled at 10 kHz and analyzed offline using pClamp10 (Axon Instruments) and Origin8 (Origin Lab) software.

Live Imaging

Conventional fluorescence and TIRF imaging was carried out under the Nikon A1R inverted microscope controlled by the Nikon NIS-Elements software. Images were acquired at 1 Hz with a 12-bit cooled EMCCD camera (Andor,

Please cite this article in press as: Shimojo et al., SNAREs Controlling Vesicular Release of BDNF and Development of Callosal Axons, Cell Reports (2015), http://dx.doi.org/10.1016/j.celrep.2015.04.032

iXon) using 10× PlanApo (N.A. 0.45), 20× PlanApo (N.A. 0.75), 60× PlanApo (N.A. 1.40), and 100× PlanApo TIRF (N.A. 1.49) objectives. Neurons were bathed in the custom-built chamber perfused at 3–4 ml/min with the NRS solution containing 10 mM HEPES-NaOH (pH 7.4), 140 mM NaCl, 5 mM KCl, 0.8 mM $MgCl_2$, 2 mM $CaCl_2$, and 10 mM glucose. The temperature was maintained at 37°C with the lens and stage heaters. Direct depolarization was induced by the application of NRS buffer in which 45 mM NaCl was substituted with KCl. Action potentials were elicited with a pair of parallel platinum electrodes connected to Model 2100 Isolated Pulse Stimulator (A-M Systems). Toxins and inhibitors were diluted in the NRS. The IP of BDNF-pHluorin-positive vesicles was measured after perfusion of de-acidification buffer composed of 10 mM HEPES-NaOH (pH 7.4), 50 mM NH_4Cl, 90 mM NaCl, 5 mM KCl, 0.8 mM $MgCl_2$, 2 mM $CaCl_2$, and 10 mM glucose.

Time-Lapse Image Data Analysis

Image stacks were aligned with TurboReg and analyzed with NIH ImageJ/Fiji plugins. Sites of activity-dependent exocytosis (e.g., regions exhibiting a rapid increase in BDNF-pHluorin or SyP-pHluorin fluorescence followed by a characteristic decay) were manually mapped in frames of a fixed size by assigning 0.8 × 0.8 μm regions of interest (ROI). P_f values were calculated as ratios of total numbers of new ENs observed prior to or during excitation to densities of internal reporter-positive vesicles that were automatically counted with FindMaxima NIH ImageJ/Fiji plugin at the end of each trial (following de-acidification with NH_4Cl). Quantifications of exocytosis in specific subcellular domains were performed in sparsely infected neurons co-expressing BDNF-pHluorin and mCherry. A detailed description of TIRF imaging is given in the Supplemental Experimental Procedures.

Statistical Analyses

Statistical analyses were performed with InStat, Prism (GraphPad), and Origin8 (Origin Lab) software. Two groups of data were subjected to Student's t test and Mann-Whitney test. Multiple groups were compared by one-way ANOVA followed by Dunnett's post hoc test or Kruskal-Wallis test.

SUPPLEMENTAL INFORMATION

Supplemental Information includes Supplemental Experimental Procedures, eight figures, two tables, and four movies and can be found with this article online at http://dx.doi.org/10.1016/j.celrep.2015.04.032.

AUTHOR CONTRIBUTIONS

A.M. and M.S. conceived the experiments. M.S. performed all studies of vesicle trafficking, secretion, and SNARE interaction. J.C. analyzed axon branching in vitro and in vivo. S.P. together with M.S. performed electrophysiological recordings. N.T.-R. and R.S. assisted with generation of expression vectors and data analysis. F.P. supervised axon branching studies. A.M. wrote the manuscript.

ACKNOWLEDGMENTS

We thank the TSRI/DNC faculty members for advice and stimulating discussions; Drs. Thomas Südhof and Martyn Goulding for providing mouse strains and antibodies; Dr. Michael Ehlers for sharing the TfR-pHluorin expression vector; Dr. Kathy Spencer for expert technical assistance; and Elisabeth Rebboah for editing the manuscript. This study was supported by the NIH grants MH085776 and NS087026 (A.M.), Novartis Advanced Discovery Institute (A.M.), The Baxter Foundation (A.M.), Japan Society for Promotion of Science (M.S.), National Institute of Mental Health Pre-doctoral National Research Service Award (R.S.), and Helen Dorris Postdoctoral Fellowship (S.P.).

Received: February 25, 2014
Revised: March 11, 2015
Accepted: April 14, 2015
Published: May 7, 2015

REFERENCES

Balkowiec, A., and Katz, D.M. (2000). Activity-dependent release of endogenous brain-derived neurotrophic factor from primary sensory neurons detected by ELISA in situ. J. Neurosci. *20*, 7417–7423.

Balkowiec, A., and Katz, D.M. (2002). Cellular mechanisms regulating activity-dependent release of native brain-derived neurotrophic factor from hippocampal neurons. J. Neurosci. *22*, 10399–10407.

Bloodgood, B.L., Sharma, N., Browne, H.A., Trepman, A.Z., and Greenberg, M.E. (2013). The activity-dependent transcription factor NPAS4 regulates domain-specific inhibition. Nature *503*, 121–125.

Cao, L., Dhilla, A., Mukai, J., Blazeski, R., Lodovichi, C., Mason, C.A., and Gogos, J.A. (2007). Genetic modulation of BDNF signaling affects the outcome of axonal competition in vivo. Curr. Biol. *17*, 911–921.

Cheng, P.L., Song, A.H., Wong, Y.H., Wang, S., Zhang, X., and Poo, M.M. (2011). Self-amplifying autocrine actions of BDNF in axon development. Proc. Natl. Acad. Sci. USA *108*, 18430–18435.

Courchet, J., Lewis, T.L., Jr., Lee, S., Courchet, V., Liou, D.Y., Aizawa, S., and Polleux, F. (2013). Terminal axon branching is regulated by the LKB1-NUAK1 kinase pathway via presynaptic mitochondrial capture. Cell *153*, 1510–1525.

Dai, H., Shin, O.H., Machius, M., Tomchick, D.R., Südhof, T.C., and Rizo, J. (2004). Structural basis for the evolutionary inactivation of Ca2+ binding to synaptotagmin 4. Nat. Struct. Mol. Biol. *11*, 844–849.

de Wit, J., Toonen, R.F., and Verhage, M. (2009). Matrix-dependent local retention of secretory vesicle cargo in cortical neurons. J. Neurosci. *29*, 23–37.

Dean, C., Liu, H., Dunning, F.M., Chang, P.Y., Jackson, M.B., and Chapman, E.R. (2009). Synaptotagmin-IV modulates synaptic function and long-term potentiation by regulating BDNF release. Nat. Neurosci. *12*, 767–776.

Dean, C., Liu, H., Staudt, T., Stahlberg, M.A., Vingill, S., Bückers, J., Kamin, D., Engelhardt, J., Jackson, M.B., Hell, S.W., and Chapman, E.R. (2012). Distinct subsets of Syt-IV/BDNF vesicles are sorted to axons versus dendrites and recruited to synapses by activity. J. Neurosci. *32*, 5398–5413.

Dieni, S., Matsumoto, T., Dekkers, M., Rauskolb, S., Ionescu, M.S., Deogracias, R., Gundelfinger, E.D., Kojima, M., Nestel, S., Frotscher, M., and Barde, Y.A. (2012). BDNF and its pro-peptide are stored in presynaptic dense core vesicles in brain neurons. J. Cell Biol. *196*, 775–788.

Fernández-Chacón, R., Königstorfer, A., Gerber, S.H., García, J., Matos, M.F., Stevens, C.F., Brose, N., Rizo, J., Rosenmund, C., and Südhof, T.C. (2001). Synaptotagmin I functions as a calcium regulator of release probability. Nature *410*, 41–49.

Geppert, M., Goda, Y., Hammer, R.E., Li, C., Rosahl, T.W., Stevens, C.F., and Südhof, T.C. (1994). Synaptotagmin I: a major Ca2+ sensor for transmitter release at a central synapse. Cell *79*, 717–727.

Giraudo, C.G., Garcia-Diaz, A., Eng, W.S., Chen, Y., Hendrickson, W.A., Melia, T.J., and Rothman, J.E. (2009). Alternative zippering as an on-off switch for SNARE-mediated fusion. Science *323*, 512–516.

Harata, N.C., Choi, S., Pyle, J.L., Aravanis, A.M., and Tsien, R.W. (2006). Frequency-dependent kinetics and prevalence of kiss-and-run and reuse at hippocampal synapses studied with novel quenching methods. Neuron *49*, 243–256.

Harms, K.J., and Craig, A.M. (2005). Synapse composition and organization following chronic activity blockade in cultured hippocampal neurons. J. Comp. Neurol. *490*, 72–84.

Holt, M., Varoqueaux, F., Wiederhold, K., Takamori, S., Urlaub, H., Fasshauer, D., and Jahn, R. (2006). Identification of SNAP-47, a novel Qbc-SNARE with ubiquitous expression. J. Biol. Chem. *281*, 17076–17083.

Johansson, J.U., Ericsson, J., Janson, J., Beraki, S., Stanić, D., Mandic, S.A., Wikström, M.A., Hökfelt, T., Ogren, S.O., Rozell, B., et al. (2008). An ancient duplication of exon 5 in the Snap25 gene is required for complex neuronal development/function. PLoS Genet. *4*, e1000278.

Jurado, S., Goswami, D., Zhang, Y., Molina, A.J., Südhof, T.C., and Malenka, R.C. (2013). LTP requires a unique postsynaptic SNARE fusion machinery. Neuron *77*, 542–558.

Kang, H., and Schuman, E.M. (1995). Long-lasting neurotrophin-induced enhancement of synaptic transmission in the adult hippocampus. Science *267*, 1658–1662.

Kerschensteiner, D., Morgan, J.L., Parker, E.D., Lewis, R.M., and Wong, R.O. (2009). Neurotransmission selectively regulates synapse formation in parallel circuits in vivo. Nature *460*, 1016–1020.

Kolarow, R., Brigadski, T., and Lessmann, V. (2007). Postsynaptic secretion of BDNF and NT-3 from hippocampal neurons depends on calcium–calmodulin kinase II signaling and proceeds via delayed fusion pore opening. J. Neurosci. *27*, 10350–10364.

Lessmann, V., Gottmann, K., and Malcangio, M. (2003). Neurotrophin secretion: current facts and future prospects. Prog. Neurobiol. *69*, 341–374.

Lu, B., Nagappan, G., Guan, X., Nathan, P.J., and Wren, P. (2013). BDNF-based synaptic repair as a disease-modifying strategy for neurodegenerative diseases. Nat. Rev. Neurosci. *14*, 401–416.

Marshak, S., Nikolakopoulou, A.M., Dirks, R., Martens, G.J., and Cohen-Cory, S. (2007). Cell-autonomous TrkB signaling in presynaptic retinal ganglion cells mediates axon arbor growth and synapse maturation during the establishment of retinotectal synaptic connectivity. J. Neurosci. *27*, 2444–2456.

Matsuda, N., Lu, H., Fukata, Y., Noritake, J., Gao, H., Mukherjee, S., Nemoto, T., Fukata, M., and Poo, M.M. (2009). Differential activity-dependent secretion of brain-derived neurotrophic factor from axon and dendrite. J. Neurosci. *29*, 14185–14198.

Maximov, A., and Südhof, T.C. (2005). Autonomous function of synaptotagmin 1 in triggering synchronous release independent of asynchronous release. Neuron *48*, 547–554.

McMahon, H.T., Ushkaryov, Y.A., Edelmann, L., Link, E., Binz, T., Niemann, H., Jahn, R., and Südhof, T.C. (1993). Cellubrevin is a ubiquitous tetanus-toxin substrate homologous to a putative synaptic vesicle fusion protein. Nature *364*, 346–349.

Miyazaki, T., Yamasaki, M., Uchigashima, M., Matsushima, A., and Watanabe, M. (2011). Cellular expression and subcellular localization of secretogranin II in the mouse hippocampus and cerebellum. Eur. J. Neurosci. *33*, 82–94.

Okawa, H., Hoon, M., Yoshimatsu, T., Della Santina, L., and Wong, R.O. (2014). Illuminating the multifaceted roles of neurotransmission in shaping neuronal circuitry. Neuron *83*, 1303–1318.

Park, H., and Poo, M.M. (2013). Neurotrophin regulation of neural circuit development and function. Nat. Rev. Neurosci. *14*, 7–23.

Patterson, S.L., Abel, T., Deuel, T.A., Martin, K.C., Rose, J.C., and Kandel, E.R. (1996). Recombinant BDNF rescues deficits in basal synaptic transmission and hippocampal LTP in BDNF knockout mice. Neuron *16*, 1137–1145.

Peng, X., Parsons, T.D., and Balice-Gordon, R.J. (2012). Determinants of synaptic strength vary across an axon arbor. J. Neurophysiol. *107*, 2430–2441.

Pieraut, S., Gounko, N., Sando, R., 3rd, Dang, W., Rebboah, E., Panda, S., Madisen, L., Zeng, H., and Maximov, A. (2014). Experience-dependent remodeling of basket cell networks in the dentate gyrus. Neuron *84*, 107–122.

Sadakata, T., Shinoda, Y., Oka, M., Sekine, Y., Sato, Y., Saruta, C., Miwa, H., Tanaka, M., Itohara, S., and Furuichi, T. (2012). Reduced axonal localization of a Caps2 splice variant impairs axonal release of BDNF and causes autistic-like behavior in mice. Proc. Natl. Acad. Sci. USA *109*, 21104–21109.

Sadakata, T., Kakegawa, W., Shinoda, Y., Hosono, M., Katoh-Semba, R., Sekine, Y., Sato, Y., Tanaka, M., Iwasato, T., Itohara, S., et al. (2013). CAPS1 deficiency perturbs dense-core vesicle trafficking and Golgi structure and reduces presynaptic release probability in the mouse brain. J. Neurosci. *33*, 17326–17334.

Sakaba, T., Stein, A., Jahn, R., and Neher, E. (2005). Distinct kinetic changes in neurotransmitter release after SNARE protein cleavage. Science *309*, 491–494.

Schoch, S., Deák, F., Königstorfer, A., Mozhayeva, M., Sara, Y., Südhof, T.C., and Kavalali, E.T. (2001). SNARE function analyzed in synaptobrevin/VAMP knockout mice. Science *294*, 1117–1122.

Sørensen, J.B., Fernández-Chacón, R., Südhof, T.C., and Neher, E. (2003a). Examining synaptotagmin 1 function in dense core vesicle exocytosis under direct control of Ca2+. J. Gen. Physiol. *122*, 265–276.

Sørensen, J.B., Nagy, G., Varoqueaux, F., Nehring, R.B., Brose, N., Wilson, M.C., and Neher, E. (2003b). Differential control of the releasable vesicle pools by SNAP-25 splice variants and SNAP-23. Cell *114*, 75–86.

Su, Q., Mochida, S., Tian, J.H., Mehta, R., and Sheng, Z.H. (2001). SNAP-29: a general SNARE protein that inhibits SNARE disassembly and is implicated in synaptic transmission. Proc. Natl. Acad. Sci. USA *98*, 14038–14043.

Südhof, T.C. (2013). Neurotransmitter release: the last millisecond in the life of a synaptic vesicle. Neuron *80*, 675–690.

Südhof, T.C., and Rothman, J.E. (2009). Membrane fusion: grappling with SNARE and SM proteins. Science *323*, 474–477.

Suh, Y.H., Terashima, A., Petralia, R.S., Wenthold, R.J., Isaac, J.T., Roche, K.W., and Roche, P.A. (2010). A neuronal role for SNAP-23 in postsynaptic glutamate receptor trafficking. Nat. Neurosci. *13*, 338–343.

Wang, C.L., Zhang, L., Zhou, Y., Zhou, J., Yang, X.J., Duan, S.M., Xiong, Z.Q., and Ding, Y.Q. (2007). Activity-dependent development of callosal projections in the somatosensory cortex. J. Neurosci. *27*, 11334–11342.

Wojcik, S.M., and Brose, N. (2007). Regulation of membrane fusion in synaptic excitation-secretion coupling: speed and accuracy matter. Neuron *55*, 11–24.

Xu, J., Mashimo, T., and Südhof, T.C. (2007). Synaptotagmin-1, -2, and -9: Ca(2+) sensors for fast release that specify distinct presynaptic properties in subsets of neurons. Neuron *54*, 567–581.

Yamasaki, S., Baumeister, A., Binz, T., Blasi, J., Link, E., Cornille, F., Roques, B., Fykse, E.M., Südhof, T.C., Jahn, R., et al. (1994). Cleavage of members of the synaptobrevin/VAMP family by types D and F botulinal neurotoxins and tetanus toxin. J. Biol. Chem. *269*, 12764–12772.

Yu, C.R., Power, J., Barnea, G., O'Donnell, S., Brown, H.E., Osborne, J., Axel, R., and Gogos, J.A. (2004). Spontaneous neural activity is required for the establishment and maintenance of the olfactory sensory map. Neuron *42*, 553–566.

Zhang, Y., Narayan, S., Geiman, E., Lanuza, G.M., Velasquez, T., Shanks, B., Akay, T., Dyck, J., Pearson, K., Gosgnach, S., et al. (2008). V3 spinal neurons establish a robust and balanced locomotor rhythm during walking. Neuron *60*, 84–96.

Cell Reports

Supplemental Information

SNAREs Controlling Vesicular Release of BDNF and Development of Callosal Axons

Masafumi Shimojo, Julien Courchet, Simon Pieraut, Nina Torabi-Rander, Richard Sando III, Franck Polleux, and Anton Maximov

Supplementary Materials for
SNAREs controlling vesicular release of BDNF and development of callosal axons

SUPPLEMENTAL FIGURE LEGENDS

Figure S1 (Related to Main Figures 1-6)

(A-D) Cultured cortical neurons were infected at 5 days *in vitro* (DIV5) with lentiviruses that drive BDNF-pHluorin under the control of either synapsin (Syn) or ubiquitin (Ub) promoter. Each virus was titrated to achieve different levels of expression (100% corresponds to undiluted stock). All experiments were performed at DIV15.

(A) Schematic diagrams of lentivirus shuttle vectors.

(B) Subcellular localization of vesicles carrying BDNF-pHluorin was assessed by confocal microscopy. Neurons were stained with antibodies to GFP (green, as a probe for BDNF-pHluorin), an axonal marker, SMI312 (red), and a somato-dendritic marker, MAP2 (blue). Representative low- and high-magnification images are shown. Scale bars apply to all experimental conditions.

(C) Total cell homogenates were probed by immunoblotting with an antibody to BDNF, which recognizes both the endogenous BDNF and BDNF-pHluorin (GFP; P=pro form; M=mature form). On the right side of the gel, different amounts of recombinant human BDNF were loaded as standards.

(D) Quantitative immunoblot analysis of expression of native BDNF and BDNF-pHluorin. $n = 3$ cultures for each condition.

(E) Subcellular distribution of vesicles carrying BDNF-pHluorin relative to markers of various organelles. Cultures were uniformly infected at DIV5 with undiluted lentiviruses that drive the expression of BDNF-pHluorin under the control of the Ub promoter. Imaging was performed following staining with antibodies to GFP (green, as a probe for BDNF-pHluorin), indicated vesicular markers (all shown in red), and MAP2 (blue). Representative images illustrate co-localization of BDNF-pHluorin with secretogranin2 and its segregation from synapsin1-positive SVs and TfR-positive recycling endosomes. Last column (on the right) shows images of wildtype neurons that were stained with antibodies to SMI312 (green) and secretogranin2.

(F) Averaged densities of vesicles with detectable BDNF-pHluorin along MAP2-positive dendrites and SMI312-positive axons. $n = 9$ neurons/group.

(G) Quantitative analysis of co-localization of BDNF-pHluorin with indicated vesicular proteins in neuronal processes. $n \geq 10$ neurons/group.

(H-J) Assessment of TrkB receptor phosphorylation and trafficking. DIV5 neurons were uniformly infected with lentiviruses that express BDNF-pHluorin, BDNF-GFP or NGF-pHluorin under the control of the Ub promoter. Experiments were performed at DIV15.

(H) Confocal imaging was carried out following labeling with antibodies to TrkB (red), GFP (green, as a probe for neurotrophin fusion proteins), and MAP2. Typical low- and high-magnification images are displayed. Scale bars apply to all sets.

(I) Total cell homogenates were probed by immunoblotting with antibodies to TrkB, phosphorylated form of TrkB, and βTubulin (as a loading standard).

(J) Left: Quantitative immunoblot analysis of TrkB expression levels, shown as a ratio of TrkB to βTubulin. Right: Averaged fractions of phosphorylated TrkB in the entire receptor pool. $n = 3$ cultures/group. Note a selective down-regulation of total TrkB levels and augmentation of receptor phosphorylation by BDNF fusion proteins.

In this and following figures, data are plotted as Mean ± S.E.M., unless specified. * denotes $p<0.05$ (defined by t-test or ANOVA).

Figure S2 (Related to Main Figures 1-6)

Cortical cultures were uniformly infected with indicated lentiviruses at DIV5 and analyzed by TIRF or conventional confocal microscopy at DIV15. All genetically-encoded fluorescent proteins were expressed under the control of the Ub promoter.

(A-G) Live neurons expressing BDNF-pHluorin were monitored under different physiological conditions. All quantifications were performed using image frames of fixed sizes that were collected in time-lapse mode with 100x PlanApo TIRF objective.

(A) Images of a region marked by a box in the wide DIC field show BDNF-pHluorin fluorescence before stimulation (Basal), during depolarization with KCl (50 mM), and following de-acidification of vesicle lumens with ammonium chloride (NH_4Cl, 50 mM). Sites of activity-dependent exocytosis are marked by yellow boxes.

(B-D) Frequencies of BDNF vesicle fusion were plotted as a function of time (10 second bin) under the normal conditions and during stimulation with 50 mM of KCl (panel **B**, green box marks the time-course of calcium rise as determined in identical settings with GCaMP3), 100 Hz action potential trains (APs, panel **C**), and GABA receptor blocker, PTX (100 μM), which promotes synaptic excitation (panel **D**).

(E) Probabilities of fusion (P_f) per minute are plotted as EN/IP ratios. Note that evoked fusion events are virtually undetectable in the presence of the membrane-impermeable hydrophilic quencher, bromophenol blue (BPB).

(F) P_f values were normalized to P_f of neurons that were depolarized with KCl.

(G) Analysis of calcium-dependence of exocytosis. Neurons were stimulated with KCl in the normal NRS solution (2 mM extracellular calcium), calcium-free NRS, or in the presence of calcium channel and NMDA receptor blockers, $CdCl_2$ (100 μM), Nifedipine (50 μM) and APV (50 μM).

(H-J) Comparative analysis of exocytosis of vesicles carrying BDNF-pHluorin and recycling endosomes (REs) that were tagged with TfR-pHluorin.

(H) Representative images show TfR-pHluorin fluorescence in dendrites of DIV15 neurons before and during KCl-induced depolarization.

(I and **J)** Mean EN and P_f before, during and after depolarization. Note that, unlike BDNF vesicles, REs exhibit robust exocytosis in the absence of external stimulation. For all quantifications, $n \geq 10$/group.

(K) Schematic representation of lentivirus shuttle vectors encoding fluorescent reporters of SVs and postsynaptic spines, tdTomato-SV2A and EBFP2-Homer1c.

(L) Neurons carrying tdTomato-SV2A (red) or EBFP2-Homer1c (blue) were stained for native synapsin1 (green) or PSD95 (red). Note that fluorescent tracers do not aggregate and overlap with endogenous synaptic proteins. A typical kymograph from triple time-lapse imaging of co-expressed BDNF-GFP, tdTomato-SV2A and EBFP2-Homer1c is shown in **Figure 1A1**.

(M and **N)** BDNF is released from both synaptic and extra-synaptic sites. BDNF-pHluorin was co-expressed and simultaneously imaged in TIRF mode with tdTomato-SV2A and EBFP2-Homer1c.

(M) Typical images illustrate the distribution of sites of KCl-induced exocytosis of BDNF vesicles (boxed in enlarged panels) relative to SV2A-positive presynaptic terminals.

(N) Quantifications of overlap of BDNF release sites with synaptic reporters. Neurons were transiently stimulated with KCl (50 mM, 2 minutes), PTX (100 μM, 2 minutes) or action potentials applied for 30 seconds at 10 and 100Hz. n = 3-5/group.

Figure S3 (Related to Main Figures 2-6)

(A-C) Distribution of intracellular peptidergic vesicles in SNARE-deficient neurons.

(A) Representative confocal images of wildtype DIV15 neurons and neurons carrying TeNT that were stained with antibodies to secretogranin2 (Sec2, red), SMI312 (green), and MAP2 (blue). Arrows mark SMI312-positive/MAP2-negative axons. A uniform infection protocol was used.

(B) Averaged densities of Sec2-positive vesicles in dendrites and axons of control and TeNT-expressing neurons. n = 10 neurons/group.

(C) Cultures were sparsely infected (as described below) with lentiviruses expressing BDNF-pHluorin and either TeNT or shRNAs against Syb2, SNAP25 and SNAP47 (KD). Infected neurons were stained for GFP (green, as a probe for reporter-positive vesicles) and MAP2 (blue). Representative low- and high-magnification confocal images show that, under all conditions, BDNF vesicles are distributed throughout the somas and processes.

(D-H) An experimental system for studies of cell-autonomous effects of SNARE loss of function.

(D) A graphic outline of culture preparation. Neurons were treated immediately after plating with a lentivirus encoding mCherry alone or together with other viruses of interest. Infected cells were then mixed at DIV1 with wildtype neurons at a 1:20 ratio, and these cultures were examined after DIV15.

(E) Schematic representation of lentivirus shuttle vectors expressing mCherry, GCaMP3 and TeNT.

(F) Typical DIC and fluorescent images of different magnification show somas, dendrites and axons of live mCherry-tagged neurons surrounded by non-infected cells (marked by asterisks in wide-field images).

(G) DIC and fluorescent images of live neurons sparsely co-expressing GCaMP3 and TeNT. Infected cells were monitored in time lapse mode before (Basal) and during augmentation of synaptic excitation with PTX (100 μM). Asterisks mark the somas of non-infected cells.

(H) Sample traces reflecting changes in intracellular calcium levels in indicated conditions, plotted as a ΔF/F0 ratio of GCaMP3 fluorescence. Note that neurons sparsely co-expressing GCaMP3 and TeNT in mixed cultures exhibit robust responses to PTX (100 μM), whereas uniform infection with TeNT completely abolishes these responses.

Figure S4 (Related to Main Figure 3)

Neurons were uniformly infected at DIV5 with lentiviruses encoding BDNF-pHluorin and two different shRNAs that target Syb/VAMP isoforms 1, 2 and 3 (target sequences are listed in **Table S1)**. Cultures were examined at DIV15-17 by immunoblotting and live TIRF imaging.

(A) Schematic diagrams of lentivirus vectors.

(B) Quantitative immunoblot analysis of pro- (P) and mature (M) BDNF levels was performed using antibodies to BDNF and βTubulin (as a loading standard). n = 6 control and Syb/VAMP-deficient cultures (examined in duplicates, KD = shRNA-mediated knockdown). Representative blots are shown in **Figure 3C.** Note a selective accumulation of mature BDNF in neurons carrying shRNAs against Syb/VAMP2.

(C) TIRF microscopy analysis of BDNF-pHluorin exocytosis. Graphs show averaged numbers of depolarization-induced fusion events (EN) and densities of intracellular reporter-positive vesicles counted after de-acidification with 50 mM of NH_4Cl (IP). Control, n = 7; Syb1 KD, n = 6; Syb2 KD, n = 7; Syb3 KD, n = 7. See also **Figure 2D-F.**

(D) Representative confocal images of wildtype neurons and neurons carrying shRNAs against Syb2 that were labeled at DIV15 with antibodies to MAP2 (blue) and Syb2 (green). Note a lack of cytotoxicity and a loss of Syb2 immunoreactivity upon KD.

(E and **F)** Cultures uniformly expressing indicated shRNAs alone (KD) or together with rescue cDNAs were examined by immunoblotting for native Syb2 and βTubulin.

(G) Quantitative immunoblot analysis of mature BDNF levels in wildtype, Syb2 KD and Syb2 KD + rescue neurons. *n* = 3 cultures/group, analyzed in duplicates using a uniform virus infection protocol.

(H-J) Subcellular localization of native Syb2.

(H) Wildtype DIV15 neurons were examined by confocal microscopy following immunostaining with antibodies to Syb2 (red), SMI312, synapsin1 and PSD95 (all in green), and MAP2 (blue). In each panel, typical images are shown at 3 different magnifications. Scale bars apply to all sets.

(I) Cultures were sparsely infected with a lentivirus that drives the expression of BDNF-pHluorin under the control of the Ub promoter. Neurons were examined by confocal microscopy at DIV15 following immunostaining with antibodies to Syb2 (red), GFP (green, as a probe for BDNF-pHluorin), MAP2, synapsin1 and PSD95 (all in blue). Scale bars apply to all sets.

(J) Quantitative analysis of co-localization of indicated proteins in wildtype neurons (images not displayed) and neurons expressing BDNF-pHluorin. *n* = 9 neurons/group.

<u>Figure S5</u> (Related to Main Figure 4)

(A and **B)** Cultures were uniformly infected at DIV5 with lentiviruses encoding BDNF-pHluorin and two different shRNAs that target SNAP isoforms 23, 25, 29 and 49 (target sequences are listed in **Table S1**). Neurons were examined at DIV15 by immunoblotting and live TIRF imaging.

(A) Quantitative immunoblot analysis of pro- (P) and mature (M) BDNF-pHluorin and native BDNF levels was performed using antibodies to BDNF and βTubulin (as a loading standard). *n* = 3 cultures (examined in duplicates, KD = shRNA-mediated knockdown). Note a selective accumulation of mature BDNF forms in neurons carrying shRNAs against SNAP25.

(B) TIRF microscopy analysis of BDNF-pHluorin exocytosis. Graphs show averaged numbers of depolarization-induced fusion events (EN) and densities of intracellular reporter-positive vesicles counted after de-acidification with 50 mM of NH_4Cl (IP). Control, *n* = 10; SNAP23 KD, *n* = 8; SNAP25 KD, *n* = 8; SNAP29 KD, *n* = 7; SNAP47 KD, *n* = 8. See also **Figure 4B-D.**

(C) Wildtype DIV15 neurons and neurons carrying shRNAs against SNAP25 or SNAP47 were labeled with antibodies to MAP2 (blue) and corresponding SNAPs (green). Typical confocal images demonstrate a lack of cytotoxicity and a loss of SNAP25/47 immunoreactivity upon KD.

(D) Neurons were uniformly infected with lentiviruses driving the expression of indicated shRNAs alone (KD) or together with rescue cDNA, and then examined by immunoblotting for native SNAP25, SNAP47 and βTubulin.

(E) Quantitative immunoblot analysis of mature BDNF levels in control, SNAP25 KD and SNAP25 KD + rescue neurons. *n* = 3 cultures/condition, analyzed in duplicates using a uniform virus infection protocol.

(F-H) Subcellular localization of native SNAPs. Cultures were sparsely infected with a lentivirus that drives the expression of BDNF-pHluorin under the control of the Ub promoter. Neurons were examined by confocal microscopy at DIV15 following immunostaining with antibodies to SNAP25/47 (both in red, panels **F** and **G**, respectively), GFP (green, as a probe for BDNF-pHluorin), MAP2, synapsin1 and PSD95 (all in blue). In each panel, typical images are shown at 3 different magnifications. Scale bars apply to all sets.

(H) Quantitative analysis of co-localization of indicated proteins in wildtype neurons and neurons expressing BDNF-pHluorin. *n* = 9 neurons/group.

Figure S6 (Related to Main Figure 4)

Kinetics of depolarization-induced exocytosis of BDNF-pHluorin was assessed by TIRF imaging in somas, dendrites and axons of sparsely infected neurons tagged with mCherry.

(A and **B)** Examples of full vesicle collapse (FC) and partial fusion (PF) in wildtype neurons. Panels illustrate decay of BDNF-pHluorin signal in two isolated sites (**A**, frames were collected every 5 seconds, arrow marks the onset of fusion) and corresponding traces of reporter fluorescence monitored in time-lapse mode (**B**, the onsets of exocytosis were digitally re-synchronized).

(C) Dual-exponential fits of averaged BDNF-pHluorin responses whose onsets and amplitudes were synchronized using a custom-made script integrated in the Origin8 software. Data were sampled from somas and dendrites of single wildtype neurons. Events were either pooled together (All) or segregated based on visual inspection followed by curve fitting. Time constants of decay are shown in inserts (e.g. 8/34 are numerical values of Tau1 and Tau2, respectively). FC: *EN*=34; PF: *EN*=149

(D) Representative images of fusion events (top panels) with corresponding kymographs (bottom panels, scale bars apply to all panels) detected in somato-dendritic domains of control neurons, and neurons expressing SNAP47 shRNA alone or with rescue cDNA.

(E) Averaged percentages of FC and PF-type fusion events in axonal and somato-dendritic compartments of control neurons.

(F) Fractions of FC and PF-type fusion events in axonal and somato-dendritic compartments of SNAP47-deficient neurons, plotted as % of control. *N*=9-10 neurons/group.

Figure S7 (Related to Main Figure 5)

DIV5 cultures were uniformly infected with lentiviruses expressing TeNT or shRNA against SNAP47. At DIV15, neurons were stained with antibodies to native synaptic proteins and subsequently examined by confocal microscopy.

(A and **B)** Typical low- and high-magnification images of neurons labeled for MAP2 (blue), synapsin1 (green) and markers of glutamatergic and GABAergic terminals, VGlut1 and VGAT (red in panels **A** and **B**, respectively).

(C) Quantitative analysis of the distribution of synapsin1, VGlut1 and VGAT-positive synapses. Average values show puncta densities along dendrites as a function of distance from cell bodies (5 μm bin). n = 15 neurons/group.

Figure S8 (Related to Main Figures 6 and 7)

(A and **B)** Subcellular distribution of SNAREs in differentiating cortical neurons in culture.

(A) Representative confocal images of wildtype DIV6 and DIV15 neurons that were labeled with antibodies to synapsin1 (red) and MAP2 (blue). Note a difference in the distribution of synapsin1 along axons (MAP2-negative processes).

(B) Wildtype DIV6 neurons were labeled for native Syb2, SNAP25 or SNAP47 (all in red) together with MAP2 (blue) and axonal markers, Tuj1 or SMI312 (both in green). Arrows mark Tuj1 and SMI312-positive axons.

(C) SNAP47 is abundant in callosal axons *in vivo.* Cortical sections were prepared from brains of P30 mice and stained with antibodies to SNAP47 (red) and MAP2 (magenta). Typical confocal images of corpus callosum and somato-sensory cortex (SSC) are shown. White arrow marks callosal axons.

(D and **E)** E15.5 embryos were *in utero* electroporated into one cortical hemisphere with mVenus tracer together with control shuttle vector or vectors encoding SNAP47 shRNA/rescue constructs.

(D) Images of the ipsi-lateral cortex in brain sections show mVenus-tagged neurons (top) and fragments of their dendrites with characteristic postsynaptic spines at P21.

(E) Quantifications of spine densities in control and SNAP47-deficient neurons. $n = 5$ mice/group.

(F and **G)** E15.5 embryos were *in utero* electroporated into one cortical hemisphere with vectors driving the expression of mVenus and shRNAs against SNAP47, BDNF or BDNF receptor, TrkB. Axon branching was examined *in vivo* at postnatal day 21. Graphs show averaged mVenus fluorescence intensities across the contralateral column. Signal was normalized to the white matter (WM, 100% defined as the maximum value). Control, $n = 11$ mice; SNAP47 KD, $n = 8$ mice; SNAP47 KD + Rescue, $n = 5$ mice. BDNF KD, $n = 3$ mice; TrkB KD, $n = 8$ mice.

Movies.

All movies were generated from time-lapse TIRF image stacks sampled at 1 Hz. The speed is 60x of actual acquisition speed. Each movie illustrates exocytosis of BDNF-pHluorin during transient depolarization with KCl (2 minutes) followed by de-acidification of internal vesicles with the buffer containing ammonium chloride. Panels are comprised of representative stacks used for quantitative analysis of EN, IP and P_f with isolated regions of detectable exocytosis (ROI) shown as inserts. Movies of BDNF exocytosis in SNARE-deficient neurons can be provided upon request.

Movie SM1 (Related to Main Figures 1-4)
Evoked exocytosis of BDNF-pHluorin followed by vesicle de-acidification in mature DIV15 neuron.

Movie SM2 (Related to Main Figures 2-4)
Evoked exocytosis of BDNF-pHluorin followed by vesicle de-acidification in soma and dendrites of mCherry-tagged DIV15 neuron in sparsely-infected culture.

Movie SM3 (Related to Main Figures 2-5)
Evoked exocytosis of BDNF-pHluorin followed by vesicle de-acidification in axons of mCherry-tagged DIV15 neuron in sparsely-infected culture.

Movie SM4 (Related to Main Figure 6)
Evoked exocytosis of BDNF-pHluorin followed by vesicle de-acidification in axons of immature mCherry-tagged DIV6 neuron in sparsely-infected culture.

Table S1. Expression vectors (Related to Main Figures 1-7)

Expression Vector	Origin	Aminoacids/Target sequence	Promoter	NCBI AN/Reference
FGW (Lentiviruses)				(Sando et al., 2012)
BDNF-GFP	Mouse	1-249 (full-length BDNF)	Ub	(Brigadski et al., 2005)
BDNF-pHluorin	Mouse	1-249 (full-length BDNF)	Ub	(Matsuda et al., 2009)
BDNF-pHluorin	Mouse	1-249 (full-length BDNF)	Syn	
NGF-pHluorin	Mouse	1-241 (full-length NGF)	Ub	NM_001112698.2
SyP-pHluroin	Mouse	1-314 (full-length Synaptophysin)	Ub	(Peng et al., 2012)
TfR-pHluroin		1-760 (full-length TfR)	Ub	(Wang et al., 2008)
tdTomato-SV2A	Rat	1-742 (full-length SV2A)	Ub	(Chang and Sudhof, 2009)
EBFP2-Homer1c	Rat	1-366 (full-length Homer1)	Ub	(Charrier et al., 2012)
GCaMP3	Synt.	1-450 (full-length GCAMP3)	Ub	HM143847
mCherry	Synt.	1-236 (full-length mCherry)	Syn	
TeNT LC	Synt.	1-455 (light chain TeNT)	Syn	L19522.1
Syb1 KD (1)	Mouse	GGACATCATGCGTGTGAAT	H1	NM_009496.3
Syb1 KD (2)	Mouse	GTGCCATCATCGTGGTAGT	H1	NM_009496.3
Syb2 KD (2)	Mouse	GTGCAGCCAAGCTCAAGCG	H1	NM_009497.3
Syb2 KD (3)	Mouse	GTGGACATCATGAGGGTGA	H1	NM_009497.3
Syb3 * KD (1)	Mouse	GATGTGGGCGATAGGGATC	H1	NM_009498.4
Syb3 KD (3)	Mouse	GGTGTTAGAAAGAGACCAG	H1	NM_009498.4
SNAP23 KD (1)	Mouse	GGAAAGAACTATAAGGCAA	H1	NM_009222.3
SNAP23 KD (2)	Mouse	CTGGAAAGCACAAGGAGAA	H1	NM_009222.3
SNAP25 KD (1)	Mouse	GCGAACAACTGGAACGCAT	H1	NM_011428.3
SNAP25 KD (2)	Mouse	GCCATATGGCTCTAGACAT	H1	NM_011428.3
SNAP25 KD (3)	Mouse	GGTTATGTTGGATGAGCAA	H1	NM_011428.3
SNAP29 KD (1)	Mouse	GCAGATTGAAAGAAGCCAT	H1	NM_023348.4
SNAP29 KD (2)	Mouse	CAGAGAAGATGGTAGACAA	H1	NM_023348.4
SNAP47 KD (1)	Mouse	GCATACGCCAGCGCTTCAT	H1	NM_144521.2
SNAP47 KD (2)	Mouse	CGATCACAGTCCTGGAGAA	H1	NM_144521.2
BDNF KD (1)	Mouse	GGTGATGCTCAGCAGTCAA	H1	NM_001048139.1
BDNF KD (2)	Mouse	CCCGGTATCCAAAGGCCAA	H1	NM_001048139.1
BDNF KD (3)	Mouse	GCCGAACTACCCAATCGTA	H1	NM_001048139.1
TrkB KD (1)	Mouse	GCGTTGACCCGGAGAACAT	H1	NM_001025074.1
TrkB KD (2)	Mouse	GTACTGGGACGTTGGGAAT	H1	NM_001025074.1
Syb2 KD/Rescue	Rat	GTGCGGCAAAACTTAAACG **	H1/Syn	NM_012663.2
SNAP25 KD/Rescue	Mouse	GCGAGCAGTTGGAGCGTAT **	H1/Syn	NM_011428.3
SNAP47 KD/Rescue	Mouse	GTATTCGGCAACGGTTCAT **	H1/Syn	NM_144521.2
Syb1-Venus	Mouse	1-118 (full-length Syb1)	Ub	NM_009496.3
Syb2-Venus	Rat	1-116 (full-length Syb2)	Ub	M24105.1
Syb3-Venus	Mouse	1-103 (full-length Syb3)	Ub	NM_009498.4
VAMP4-Venus	Mouse	1-141 (full-length VAMP4)	Ub	AK018344.1
VAMP5-Venus	Mouse	1-102 (full-length VAMP5)	Ub	NM_016872.4
VAMP7-Venus	Mouse	1-220 (full-length VAMP7)	Ub	NM_011515.4
VAMP8-Venus	Mouse	1-101 (full-length VAMP8)	Ub	NM_016794.3
YKT6-Venus	Mouse	1-198 (full-length YKT6)	Ub	NM_019661.4
Sec22b-Venus	Mouse	1-215 (full-length Sec22b)	Ub	NM_011342.4
SNAP23-Venus	Mouse	1-210 (full-length SNAP23)	Ub	NM_009222.3
SNAP25-Venus	Mouse	1-206 (full-length SNAP25)	Ub	NM_011428.3
SNAP29-Venus	Mouse	1-260 (full-length SNAP29)	Ub	NM_023348.4
SNAP47-Venus	Mouse	1-413 (full-length SNAP47)	Ub	NM_144521.2
pSCV2 backbone				
mVenus	Synt.	Full-length monomeric Venus	CAG	(Courchet et al., 2013)

* Syb3 is also known as Cellubrevin. ** Silent mutations that disable RNA interference are shown in red.

Table S2. Synaptic transmission in cultured Syb2, SNAP25- and SNAP47-deficeint cortical neurons (Related to Main Figure 5)

	Mean +/- S.E.M.	*n***	P value***
Evoked EPSC amplitude (nA)			
Control	1.0 +/- 0.2	13	
TeNT	0.13 +/- 0.04	11	<0.001
SNAP47 KD*	1.1 +/- 0.2	13	0.51
SNAP47 KD + Rescue	1.1 +/- 0.02	10	0.64
Evoked IPSC amplitude (nA)			
Control	3.6 +/- 0.4	19	
TeNT	0.05 +/- 0.03	3	<0.001
Syb2 KD*	0.3 +/- 0.1	5	<0.001
SNAP25 KD	2.0 +/- 0.5	12	0.01
SNAP47 KD	3.3 +/- 0.3	14	0.44
SNAP47 KD + Rescue	3.8 +/- 0.6	10	0.68

*KD = shRNA-mediated knock-down.
***n* = total number of neurons analyzed; each synaptic parameter was examined in at least two independent neuronal culture preparations.
*** P values (experimental versus control group).

EXTENDED METHODS

Reagents. The following commercial polyclonal and monoclonal antibodies were used for immunocytochemistry and immunoblotting: anti-BDNF (Santa Cruz, N20, sc-546); anti-Cux1 (Santa Cruz, M-222, sc13024); anti-βTubulin III (Sigma, T2200); anti-SMI312 (Covance, SMI-312R); anti-MAP2 (Sigma, clone HM2, M4403); anti-MAP2 (Millipore, clone AP20, MAB3418); anti-MAP2 (Millipore, AB5622); anti-TrkB (Millipore, 07-225); anti-vGluT1 (Millipore, AB5905); anti-phosphoTrk (Cell Signaling, 4621); anti-GFP (AVES, GFP-1020); anti-SNAP47 (SySy, 111 403); anti-VGAT (SySy, 131 003); anti-Synaptobrevin2 (SySy, 104 211); anti-SNAP25 (SySy, 111 011); anti-Synapsin (SySy, 106 011); anti-SecII (Biodesign International, K5510R); Other antibodies were a kind gift of Dr. Thomas Südhof. Toxins and inhibitors were purchased from Tocris or Sigma and used at the following concentrations: APV (Cat# 01061, 50 μM), CNQX (Cat# 01045, 10 μM), Picrotoxin (Cat# 1128, 100 μM), Tetrodotoxin (Cat# 50809813, 1 μM).

Mice. Wildtype mice of a mixed 129SvJ/C57BL/6J background were used for preparation of neuronal cultures and immunoprecipitations. *In utero* electroporations were performed in wildtype F1-hybrid females resulting of the cross between inbred C57BL/6J and 129SvJ parents. *CamKIIα*:Cre and $R26^{\text{floxstop-TeNT}}$ alleles were described previously (Sando et al., 2012; Zhang et al., 2008). Animals were housed and analyzed according to the protocols approved by the IACUC committee.

Plasmid construction. Coding sequences were inserted into previously characterized FGW shuttle vector that contains recombination arms, a flap HIV-1 sequence, a multiple cloning site, and a WRE element (Maximov et al., 2009; Sando et al., 2013; Sando et al., 2012). Expression of cDNAs and shRNAs was driven by the Ubiquitin (Ub, Pol II), Synapsin (Syn, Pol II) and H1 (Pol III) promoters. Knockdown/rescue studies were carried out with vectors containing Syn and H1 promoters in the same backbone. These constructs were used to produce recombinant lentiviruses in HEK293 cells and for *in utero* electroporation

(as plasmid DNA). For TeNT cleavage assays, shuttles driving the expression of GFP-tagged SNAREs and untagged TeNT under the control of the Ub promoter were transiently transfected into HEK293 cells. Sequences encoding BDNF-pHluorin, BDNF-GFP (Venus), SyP-pHluorin and TeNT were described previously (Brigadski et al., 2005; Matsuda et al., 2009; Peng et al., 2012; Sando et al., 2013), and were a kind gift of Dr. Thomas Südhof. To generate pre- and postsynaptic markers with non-overlapping excitation/emission spectra, two well-characterized reporters, EGFP-SV2A and EGFP-Homer1c (Chang and Sudhof, 2009; Charrier et al., 2012) were modified by replacing EGFP with tdTomato and EBFP2, respectively. The appropriate sorting of these markers to synapses was confirmed by co-labeling of mature neurons for native synapsin1 and PSD95. GCaMP3 and mCherry were a kind gift of Dr. Ulrich Mueller. TfR-pHluorin was a kind gift of Dr. Michael Ehlers. All other cDNAs were amplified by PCR using embryonic mouse brain cDNA library as a template.

Design and validation of vectors expressing shRNAs. Synthetic oligonucleotides encoding hairpins were inserted into XhoI/XbaI sites immediately downstream of the H1 promoter. All constructs were verified by sequencing prior to use. shRNAs were initially pre-screened in cultured neurons by lentiviral co-expression with corresponding GFP-tagged cDNAs to meet three criteria, as determined by live GFP imaging, detection of native proteins, and immunostaining for common neuronal and synaptic markers: i) high potency of knock-downs (>90%); ii) lack of cross-reactivity with mRNAs of homologous genes; and iii) lack of cytotoxicity. Validated shRNAs were then co-expressed in duplicates, and the effects of knockdowns on BDNF levels and efficacy of vesicle exocytosis were assessed by immunoblotting and TIRF microscopy. Subsequently, one shRNA per each candidate SNARE was used to generate dual-promoter rescue vectors harboring cDNAs with silent non-coding mutations that disable RNA interference. See **Table S1** below for additional sequence information and NCBI database accession numbers (ANs). Full vector NTI maps can be provided upon request.

TIRF imaging. We chose to image BDNF-pHluorin by TIRF microscopy since no fast readouts for release of native BDNF exist. This method enables monitoring exocytosis with high temporal and spatial resolution, and diminishes artifacts associated with occasional fluctuations of reporter fluorescence in internal vesicles. We used the published protocol (Matsuda et al., 2009) with several modifications. BDNF-pHluorin was introduced into primary neurons in dissociated cultures with low densities of astrocytes (2-3%) to avoid interference from glia that often resides between neurons and glass interface. Our pilot experiments indicated that relatively high BDNF-pHluorin copy numbers per vesicle are necessary for reliable detection of fusion events. To ensure that overexpression does not result in abnormal vesicular sorting, we systematically examined the processing and subcellular distribution of BDNF-pHluorins that were introduced with lentiviruses of various titers and under the control of the ubiquitin (Ub) or synapsin (Syn) promoters of different strength (**Figure S1A**). Neurons were infected at 5 days *in vitro* (DIV5) and analyzed by immunoblotting and immunostaining at DIV15, when they establish polarized morphologies with abundant synaptic connectivity. In all cases, recombinant proteins were cleaved into mature forms, and were sorted into vesicles that enter SMI312-positive axons and MAP2-positive dendrites (**Figure S1B-D**). Further analysis of neurons expressing BDNF-pHluorin from a stronger Ub promoter showed that 70-80% of reporter-containing vesicles were immunoreactive for a native marker of peptigergic vesicles, secretogranin2. In contrast, these organelles were largely segregated from markers of presynaptic boutons, postsynaptic spines, as well as TfR-positive recycling endosomes that are thought to mediate the membrane

insertion of postsynaptic AMPA receptors during long-term potentiation (**Figures S1E** and **S1G**). Lastly, BDNF-pHluorin but not NGF-pHluorin promoted the phosphorylation and degradation of native TrkB receptors without producing apparent changes in receptor localization (**Figure S1H-J**). Taken together, these results suggest that mis-targeting of the reporter was unlikely.

All TIRF imaging studies were performed with a 100x PlanApo TIRF (N.A. 1.49) objective. We calibrated the perfusion system by determining the time-course of KCl-induced calcium rise in neurons carrying GCaMP3. Additional control experiments were performed to ensure that, similar to native BDNF, BDNF-pHluorin is secreted in an activity- and calcium-dependent manner and that observed changes in reporter fluorescence reflect vesicle fusion with the plasma membrane (**Figure S2A-G**). Side-by-side analysis of BDNF-pHluorin, SyP-pHluotin, and TfR-pHluorin revealed drastic differences in spatial and temporal dynamics of exocytosis, which further rules out the possibility of non-specific targeting of reporters into all vesicle types (**Figures 1D-E** and **S2H-J**).

Our strategies for quantitative analysis of exocytosis and data representation were devised to take into consideration the following: i) Desynchronized nature of BDNF release. Because fusion events occur at different times during neuronal excitation, we present event maps and real-time traces that reflect exocytosis in each site; ii) Potential fluctuation in neuron and vesicle density across different experiments. We took this into account by calculating the total numbers of new events (EN) that appear during fixed time intervals, numbers of internal reporter-positive vesicles counted after de-acidification (intracellular pool, IP) and probability of fusion (P_f=EN/IP). We also plot averaged EN as a function of time using 10 second bins, since the frequency of exocytosis is relatively low even during robust stimulation; iii) Potential fluctuation in BDNF-pHluorin expression levels and pH of the bath solution across independent experiments. Both factors affect the peak amplitudes of reporter response during exocytosis ($\Delta F/F0$). We therefore exclusively test the effects of SNARE loss-of-function on EN, IP, P_f and kinetics of decay, and do not compare peak amplitudes.

In live imaging studies with sparsely infected neurons, axons, dendrites and somas were distinguished by mCherry reporter expression. We validated this approach by performing immunostaining of mCherry-tagged neurons with markers of axonal and somato-dendritic compartments, SMI312 and MAP2. To further avoid contamination with events that arise from intermingled processes of neighboring cells, frames for high-resolution TIRF imaging were first selected at low magnification for areas of distal axon segments or somas with proximal dendrites. We did not image distal dendrites since they can be confused with axons. Because TIRF imaging of BDNF-pHluorin can only be performed at high magnification, we were unable to simultaneously monitor exocytosis from the entire surface of a neuron. Thus, raw EN measurements only reflect isolated segments of axons and the total numbers of fusion events per cell are actually larger. Nevertheless, this problem is alleviated by measurements of P_f. It is also essential to note that, during imaging of mixed cultures, many axons of BDNF-pHluorin-expressing neurons were present in each field of view as opposed to axons of single mCherry-tagged neurons. Therefore, EN values calculated in axons and dendrites of individual neurons cannot be summed for direct comparison with values obtained from mixed cultures.

For analysis of vesicle fusion kinetics (**Figure S6**), single traces of BDNF-pHluorin fluorescence were sampled from sparsely infected mCherry-tagged neurons. These traces were digitally re-synchronized using a custom-made script developed in collaboration with the Origin Lab. Consistent with previous work

(Matsuda et al., 2009), we found that BDNF vesicles fuse with the plasma membrane in two modes: full vesicle collapse (FC) and partial fusion (PF) pore opening. PF and FC-type events were segregated using the following criteria: events decaying by >75% within 15 seconds were considered FC. The remaining slowly decaying events were counted as PF. All multi-peak events were excluded from these quantifications. Decay time constants were determined by double-exponential fitting with the following formula: $y = y_0 + A_1e^{-x/t1} + A_2e^{-x/t2}$. In wildtype neurons, ~80% ($p<0.01$) of fusion events resembled PF vesicles that gradually secrete cargo after the onset of exocytosis, resulting in a slow decay of reporter fluorescence (**Figure S6A-C** and **S6E**). KD of SNAP47 only suppressed the PF mode in axons, while the remaining rapidly decaying FC-type events were abolished in all subcellular domains (**Figure S6D-F**). Given the relatively low frequency of FC, it is not surprising that this shift towards PF could not be revealed by our initial quantifications of total EN and P_f in somas and dendrites. On the contrary, KDs of Syb2 and SNAP25 had a tendency to abolish both fusion modes, albeit the small number of events available for quantification precluded us from obtaining sufficient statistical power (data not shown). Therefore, SNAP47 predominantly controls the bulk exocytosis of BDNF in axons, while promoting the full vesicle collapse across somas and processes.

Owning to its many roles in synaptic plasticity, BDNF is widely believed to be secreted at synapses (Edelmann et al., 2014; Park and Poo, 2013). Yet, the experimental evidence supporting this hypothesis is largely based on imaging studies with cultured neurons where overexpressed BDNF-GFP or BDNF-pHluorin were observed to overlap with markers comprised of synaptic proteins fused to mCherry or dsRed (Brigadski et al., 2005; Kolarow et al., 2007; Shinoda et al., 2011). In our hands, all mCherry- and dsRed-tagged synaptic proteins (but not mCherry alone) aggregated in somas, axons and dendrites, suggesting these markers cannot be used for reliable analysis of co-localization (these images can be provided upon request). We detected significant aggregation even when mCherry and dsRed fusions were assembled following strategies that produce satisfactory results with EGFP, Venus, YFP and CFP. We selected tdTomato-SV2A and EBFP2-Homer1c after extensive screening for reliable markers whose excitation/emission spectra do not overlap with BDNF-pHluorin, and confirmed appropriate targeting of these fusions by co-staining neurons with antibodies to other native pre- and postsynaptic proteins (these data can be provided upon request). In fact, our observation that many BDNF release sites are segregated from synapses is not surprising. Indeed, the exocytosis of BDNF does not appear to require compartmentalized active zones and postsynaptic spines, considering that even immature differentiating neurons exhibit a robust release of native BDNF and BDNF-pHluorin in response to excitation (**Figure 6A-C**) (Balkowiec and Katz, 2000; Cheng et al., 2011).

Analysis of axon branching in vitro. Shuttle vectors encoding shRNA without or with rescue cDNA (1 μg/ml) were mixed with 1% Fast Green (Sigma) and pSCV2-mVenus plasmid. These mixtures were injected into the lateral ventricles of E15.5 embryos of time-pregnant mice followed by electroporation as previously described (Courchet et al., 2013). Immediately after electroporation, the cortices were isolated in HBSS supplemented with 1 mM HEPES-NaOH, pH7.4 and glucose and digested with papain (Worthington) and DNase (Sigma). Dissociated cells were plated onto poly-D-Lysine and laminin (Sigma) coated glass coverslips at a density of 35,000-50,000cells/cm^2. Cultures were fixed at DIV5 and the mVenus fluorescence was enhanced by immunostaining for GFP followed by labeling with Alexa488 secondary antibody. Axons and dendrites were distinguished based on characteristic morphology and by

staining with antibodies to axonal and somato-dendritic markers, SMI312 and MAP2. The numbers of axon branches in each isolated neuron were measured using Nikon NIS-elements and Simple Neurite Tracer plugins. Recombinant human BDNF (Sigma) was daily added to the culture medium starting at DIV1 a concentration of 50 ng/ml.

Analysis of axon branching in vivo was performed using published protocols (Courchet et al., 2013). Briefly, E15.5 embryos were electroporated *in utero* with a mixture of plasmids as describe above. At postnatal day 21, mice were anesthetized and sacrificed by terminal perfusion of 4% paraformaldehyde. Brains were post-fixed in 4% PFA for 2 hours at room temperature. 100 μm free-floating coronal slices (including the corpus callosum) were cut with a vibratome VT1200S (Leica). Sections were subsequently blocked and permeabilized in the PBS buffer containing 1% BSA and 0.2 % Triton X-100 followed by treatments with primary and secondary antibodies to enhance the mVenus signal. Nuclei were labeled with Hoechst 33258 (Pierce). Samples were mounted on slides and imaged under a Nikon C2 confocal microscope.

Miscellaneous. For quantitative immunoblot analysis of BDNF levels, intensities of chemiluminescent signals were measured with ImageJ software using calibration curves obtained with synthetic human BDNF (Almone Lab) and mouse brain lysate.

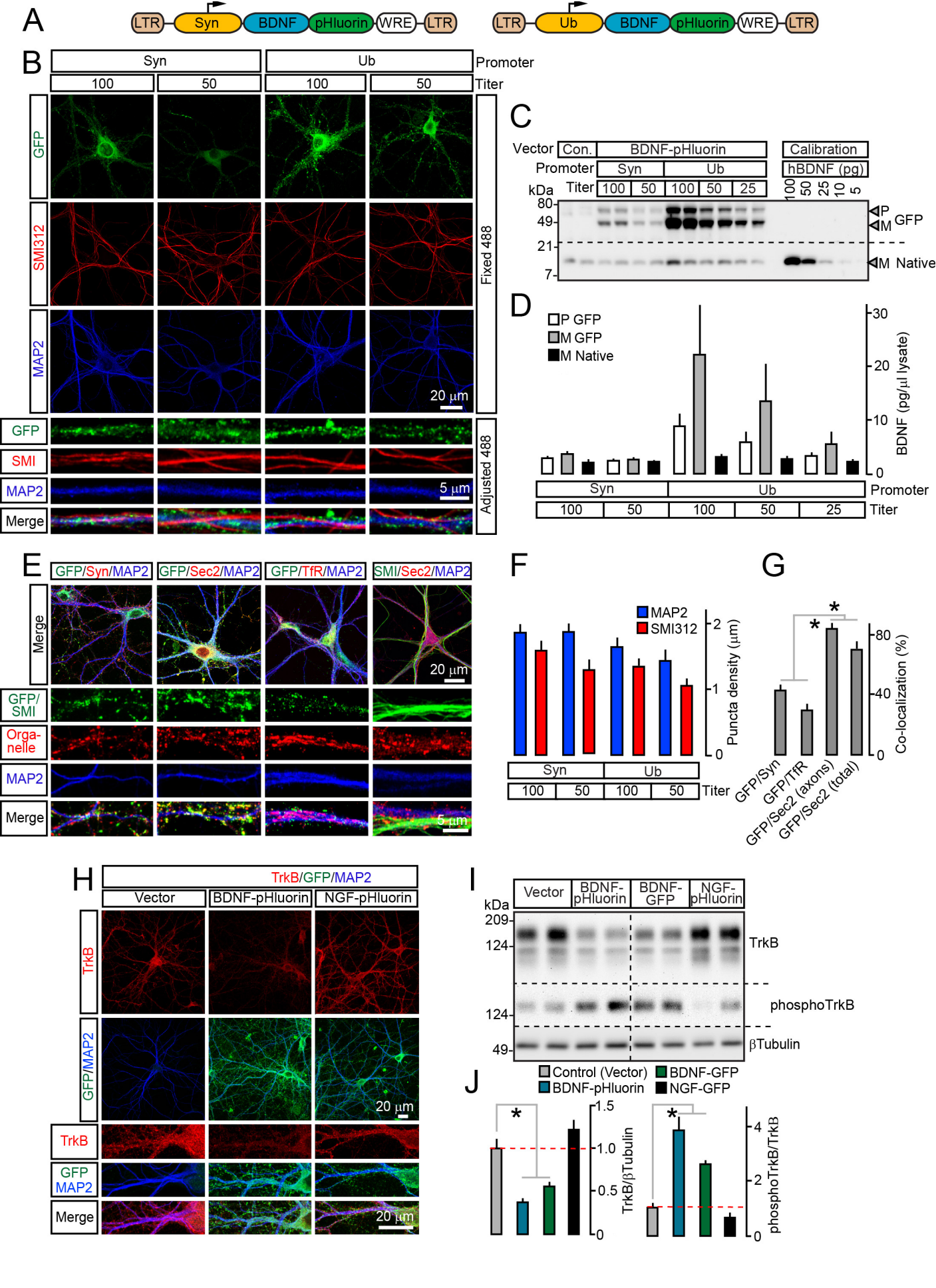

Fig. S1 Shimojo et al

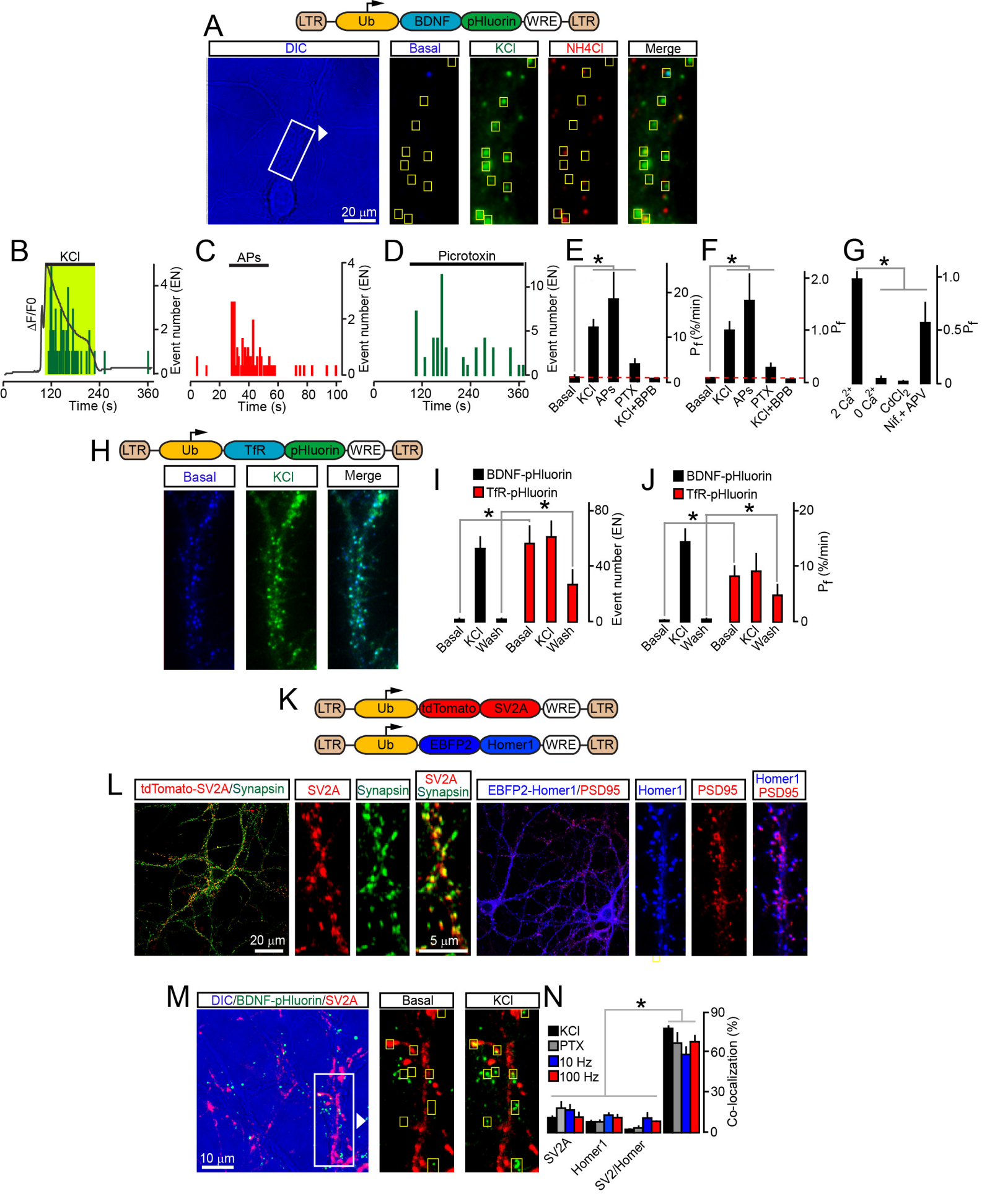

Fig. S2 Shimojo et al

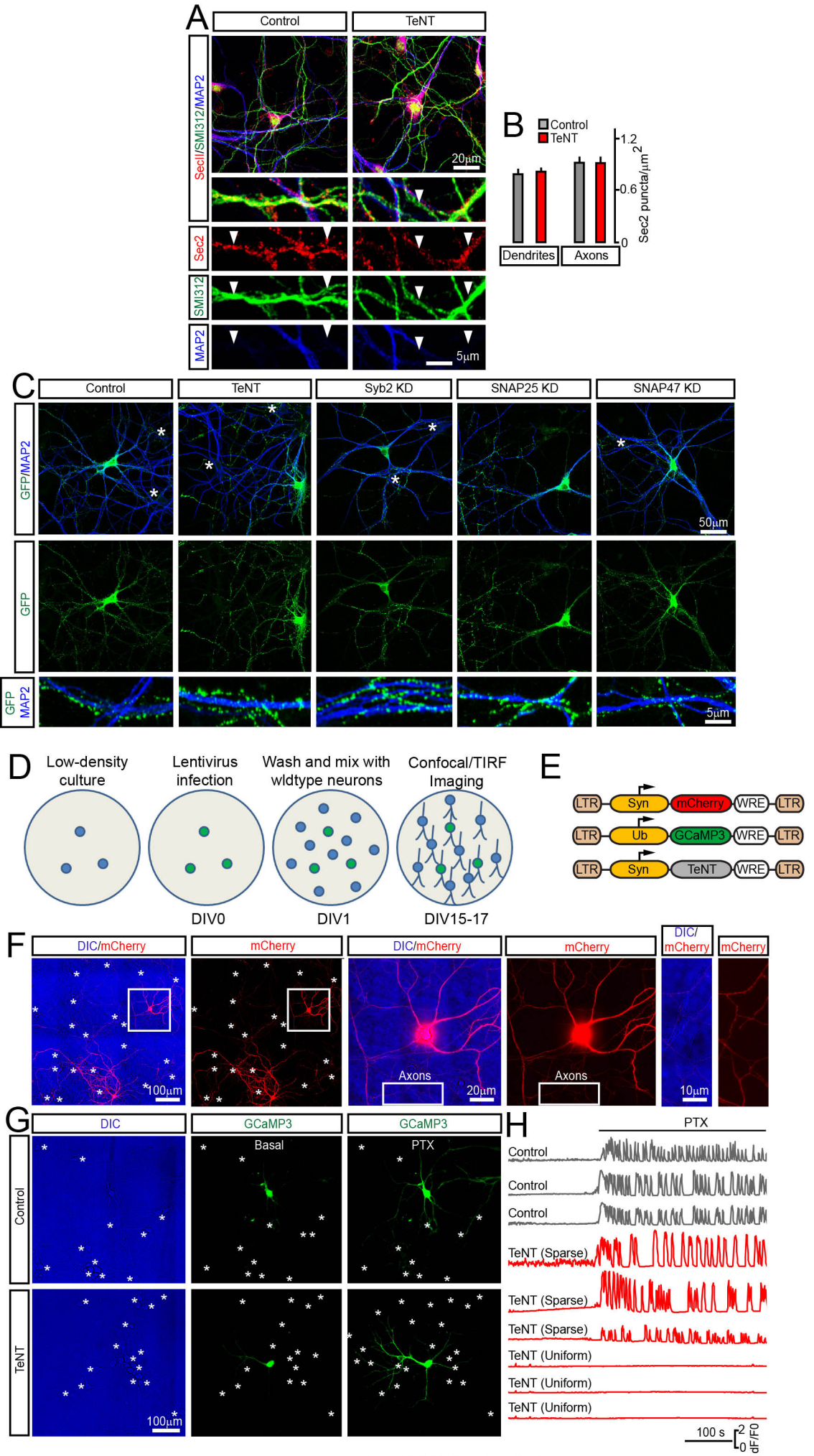

Fig. S3 Shimojo et al

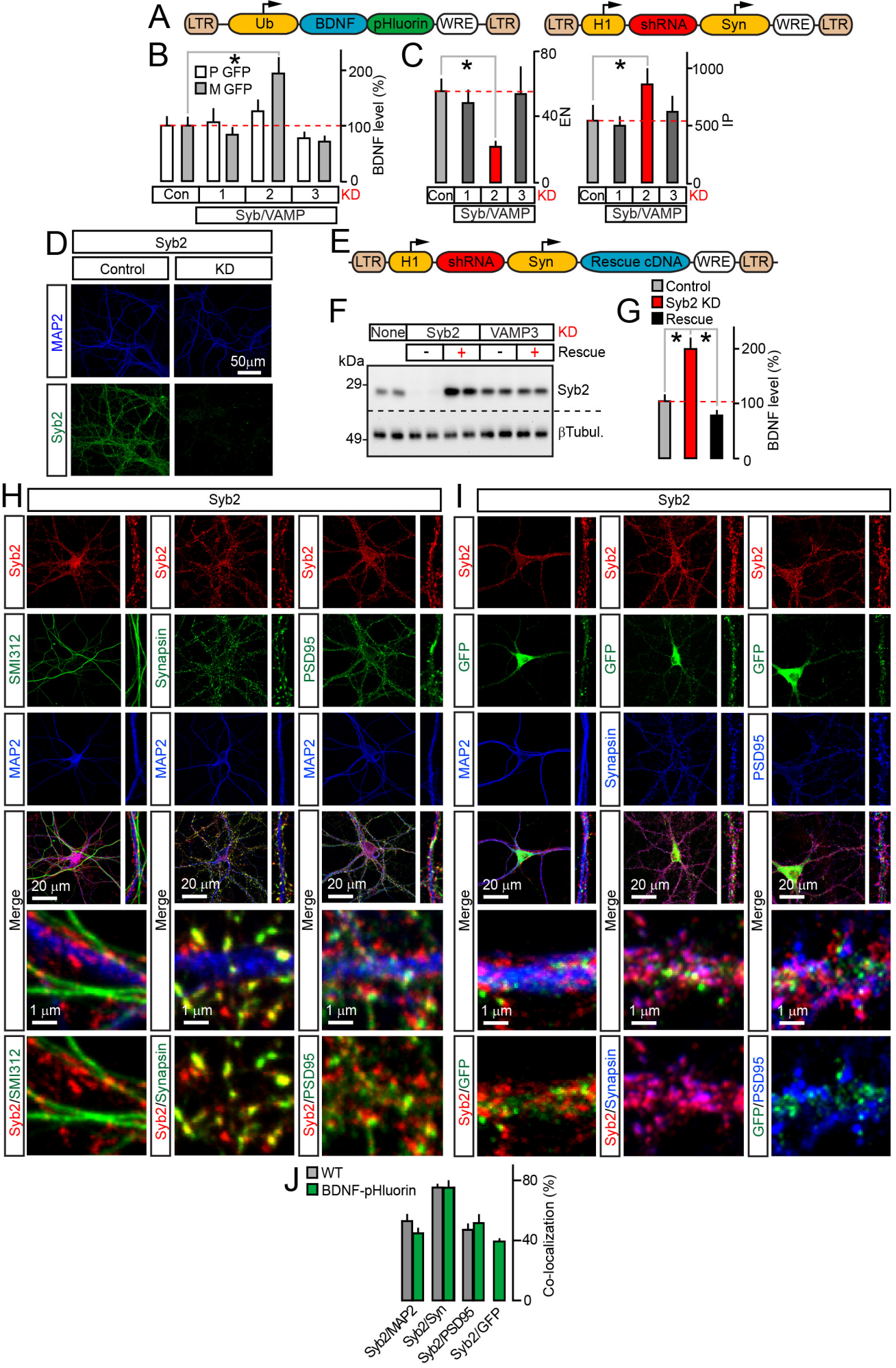

Fig. S4 Shimojo et al

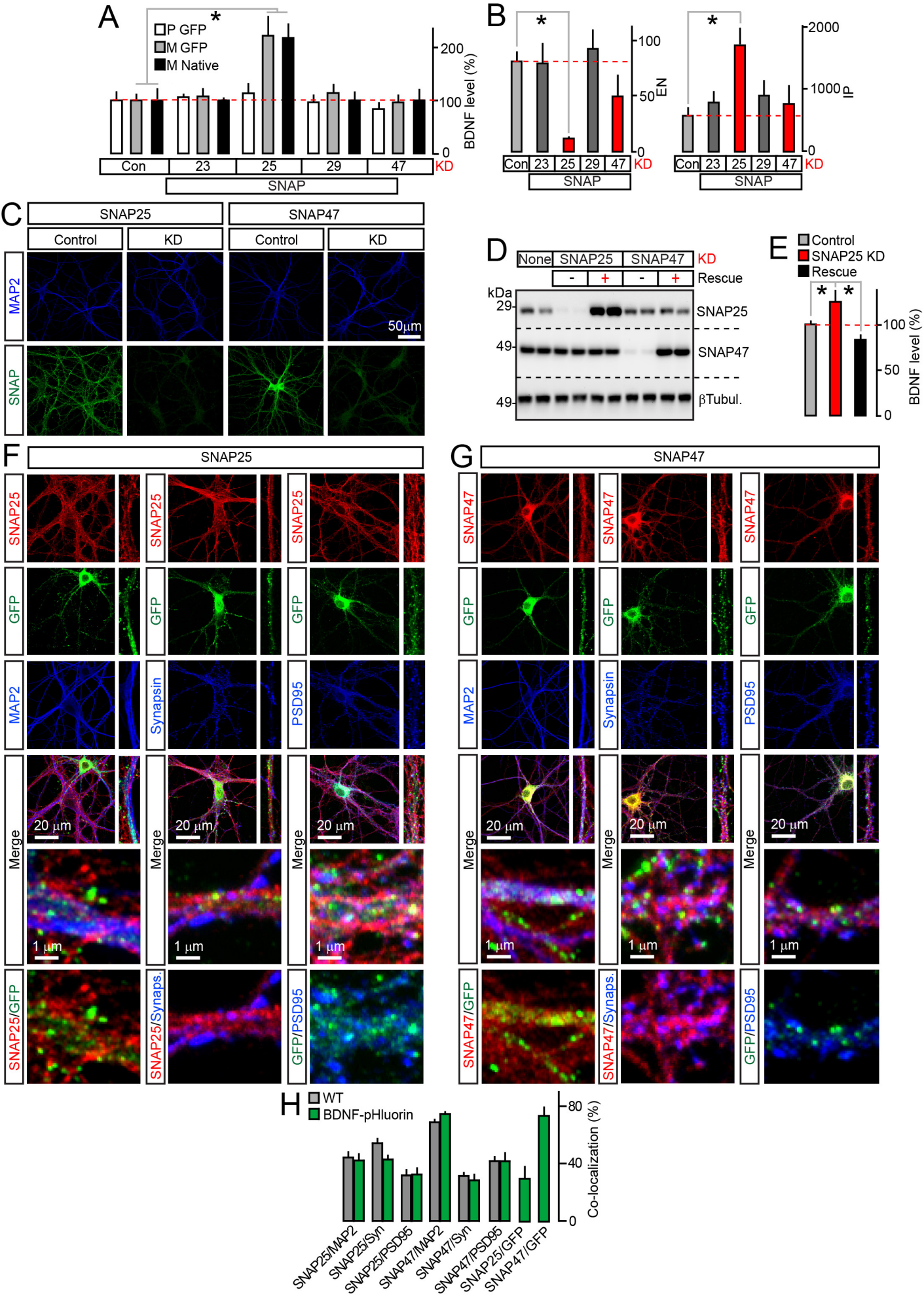

Fig. S5 Shimojo et al

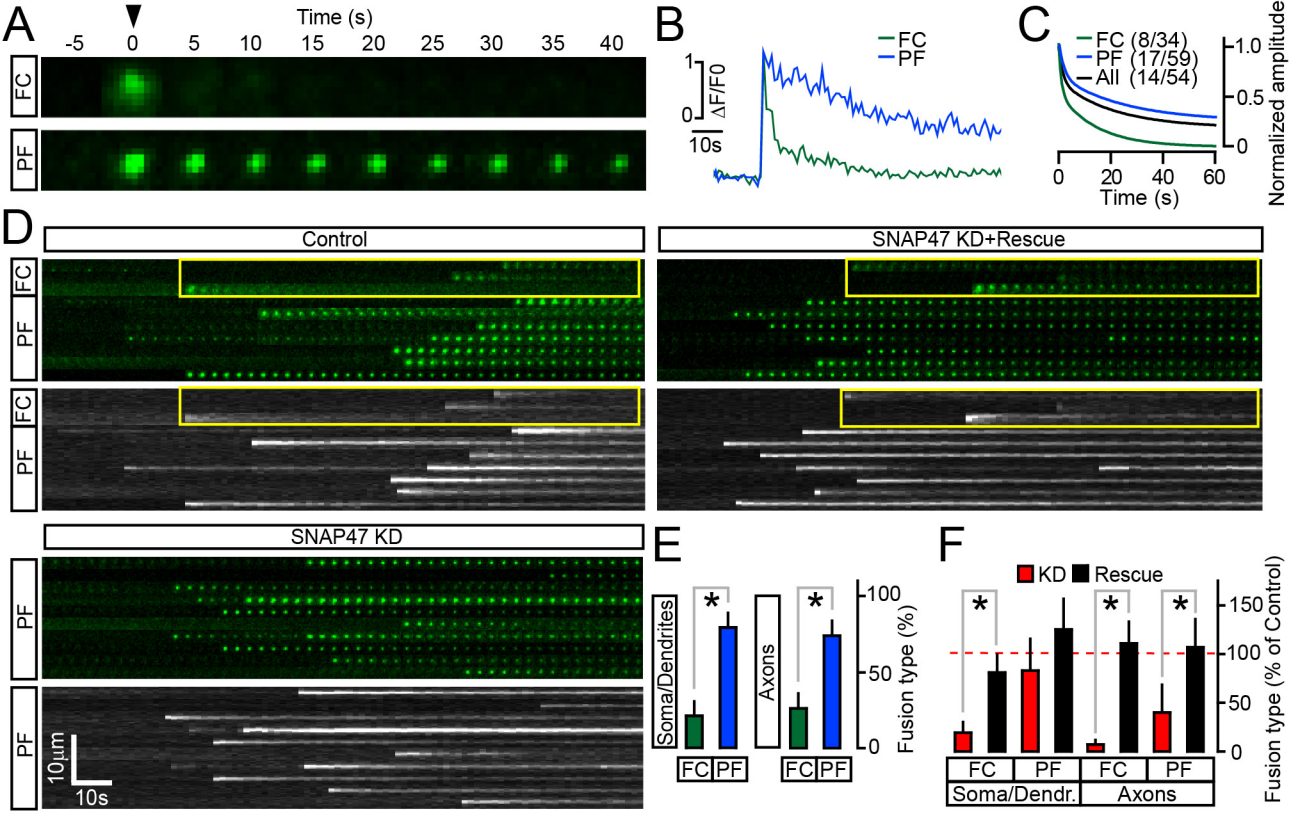

Fig. S6 Shimojo et al

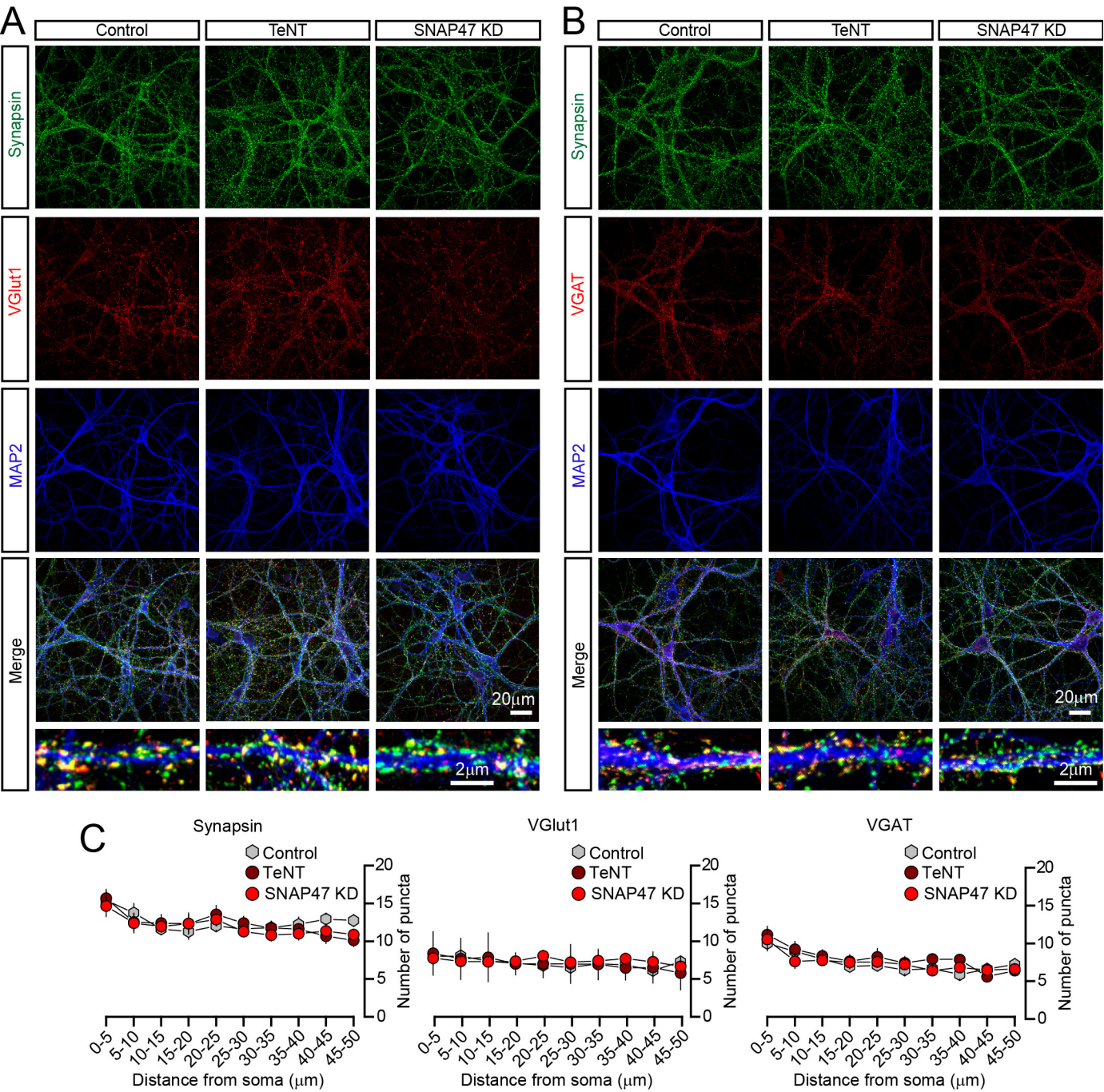

Fig. S7 Shimojo et al

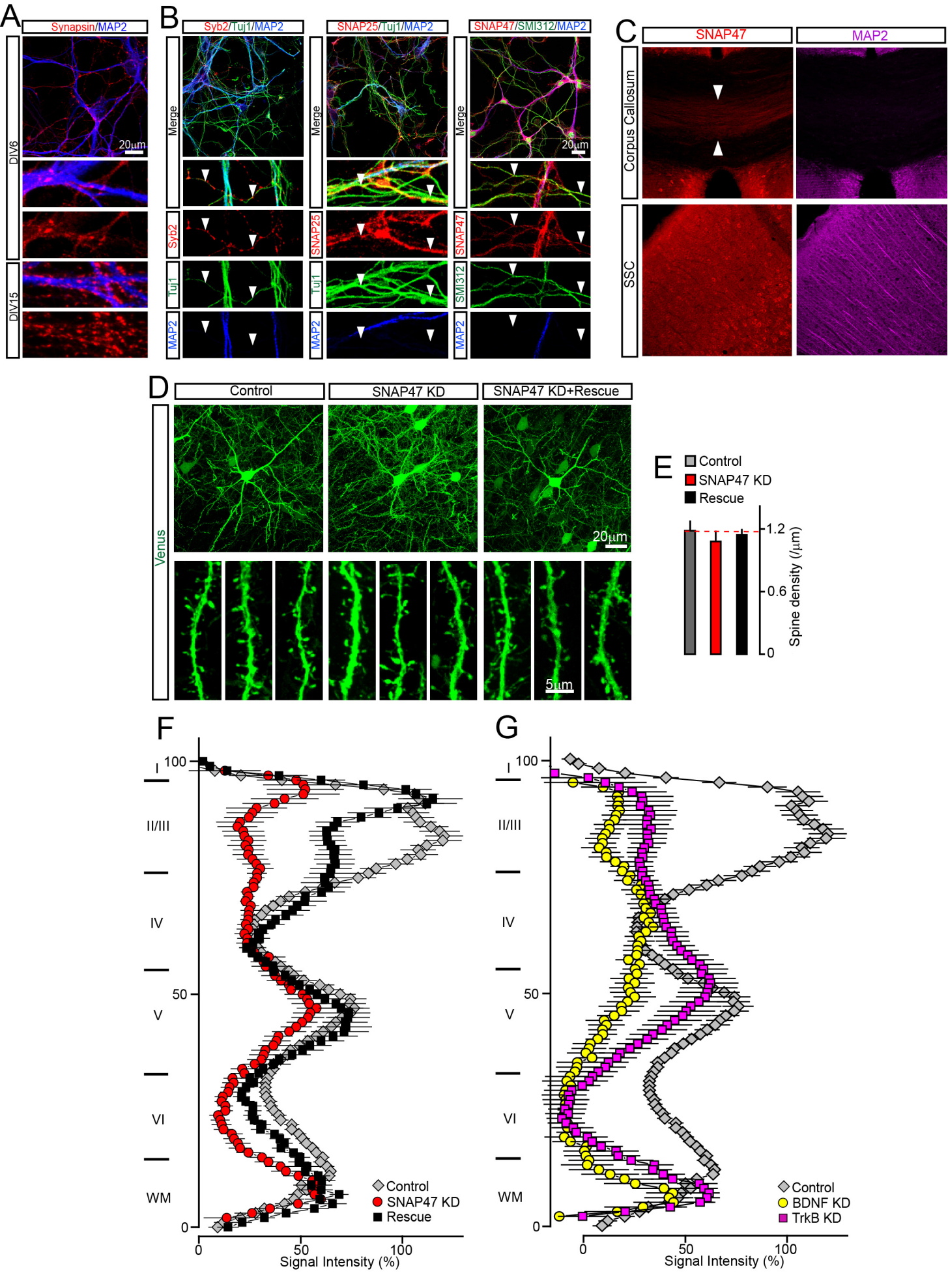

Fig. S8 Shimojo et al